

The GAPS Programme with HARPS-N at TNG

XVIII. Two new giant planets around the metal-poor stars HD 220197 and HD 233832 ^{*}

D. Barbato^{1,2}, A. Sozzetti², K. Biazzo³, L. Malavolta^{4,5}, N.C. Santos^{6,7}, M. Damasso², A.F. Lanza³, M. Pinamonti², L. Affer⁸, S. Benatti⁵, A. Bignamini⁹, A.S. Bonomo², F. Borsa¹⁰, I. Carleo^{5,4}, R. Claudi⁵, R. Cosentino¹¹, E. Covino¹², S. Desidera⁵, M. Esposito^{12,13}, P. Giacobbe², E. González-Álvarez⁸, R. Gratton⁵, A. Harutyunyan¹¹, G. Leto³, A. Maggio⁸, J. Maldonado⁸, L. Mancini^{14,15,2}, S. Masiero⁸, G. Micela⁸, E. Molinari^{11,16}, V. Nascimbeni^{4,5}, I. Pagano³, G. Piotto^{4,5}, E. Poretti^{11,10}, M. Rainer^{10,17}, G. Scandariato³, R. Smareglia⁹, L.S. Colombo⁴, L. Di Fabrizio¹¹, J.P. Faria^{6,7}, A. Martinez Fiorenzano¹¹, M. Molinaro⁹, and M. Pedani¹¹

¹ Dipartimento di Fisica, Università degli Studi di Torino, via Pietro Giuria 1, I-10125 Torino, Italy

² INAF – Osservatorio Astrofisico di Torino, Via Osservatorio 20, I-10025 Pino Torinese, Italy

³ INAF – Osservatorio Astrofisico di Catania, Via S. Sofia 78, I-95123, Catania, Italy

⁴ Dipartimento di Fisica e Astronomia "G. Galilei", Università di Padova, Vicolo dell'Osservatorio 3, I-35122 Padova, Italy

⁵ INAF – Osservatorio Astronomico di Padova, Vicolo dell'Osservatorio 5, I-35122, Padova, Italy

⁶ Instituto de Astrofísica e Ciências do Espaço, Universidade do Porto, CAUP, Rua das Estrelas, 4150-762 Porto, Portugal

⁷ Departamento de Física e Astronomia, Faculdade de Ciências, Universidade do Porto, Rua do Campo Alegre, 4169-007 Porto, Portugal

⁸ INAF – Osservatorio Astronomico di Palermo, Piazza del Parlamento 1, I-90134, Palermo, Italy

⁹ INAF – Osservatorio Astronomico di Trieste, via Tiepolo 11, I-34143 Trieste, Italy

¹⁰ INAF – Osservatorio Astronomico di Brera, Via E. Bianchi 46, I-23807 Merate (LC), Italy

¹¹ Fundación Galileo Galilei - INAF, Rambla José Ana Fernández Pérez 7, E-38712 Breña Baja, TF, Spain

¹² INAF – Osservatorio Astronomico di Capodimonte, Salita Moiariello 16, I-80131, Napoli, Italy

¹³ Thüringer Landessternwarte Tautenburg, Sternwarte 5, D-07778 Tautenburg, Germany

¹⁴ Dipartimento di Fisica, Università di Roma Tor Vergata, Via della Ricerca Scientifica 1, 00133 Roma, Italy

¹⁵ Max Planck Institute for Astronomy, Königstuhl 17, 69117 Heidelberg, Germany

¹⁶ INAF – Osservatorio Astronomico di Cagliari, Via della Scienza 5, I-09047 Selargius (CA), Italy

¹⁷ INAF – Osservatorio Astrofisico di Arcetri, Largo E. Fermi 5, I-50125 Firenze, Italy

Received <date> / Accepted <date>

ABSTRACT

Context. Statistical studies of exoplanets have shown that giant planets are more commonly hosted by metal-rich dwarf stars than low-metallicity ones, while such a correlation is not evident for lower-mass planets. The search for giant planets around metal-poor stars and the estimate of their occurrence f_p is an important element in providing support to models of planet formation.

Aims. We present results from the HARPS-N search for giant planets orbiting metal-poor ($-1.0 \leq [\text{Fe}/\text{H}] \leq -0.5$ dex) stars in the northern hemisphere complementing a previous HARPS survey on southern stars in order to update the estimate of f_p .

Methods. High-precision HARPS-N observations of 42 metal-poor stars are used to search for planetary signals to be fitted using differential evolution MCMC single-Keplerian models. We then join our detections to the results of the previous HARPS survey on 88 metal-poor stars to provide a preliminar estimate of the two-hemisphere f_p .

Results. We report the detection of two new giant planets around HD 220197 and HD 233832. The first companion has $M \sin i = 0.20^{+0.07}_{-0.04} M_{\text{Jup}}$ and orbital period of 1728^{+162}_{-80} days, and for the second companion we find two solutions of equal statistical weight having periods 2058^{+47}_{-40} and 4047^{+91}_{-117} days and minimum masses of $1.78^{+0.08}_{-0.06}$ and $2.72^{+0.23}_{-0.23} M_{\text{Jup}}$, respectively. Joining our two detections with the three from the southern survey we obtain a preliminar and conservative estimate of global frequency of $f_p = 3.84^{+2.45}_{-1.06}\%$ for giant planets around metal-poor stars.

Conclusions. The two new giant planets orbit dwarf stars at the metal-rich end of the HARPS-N metal-poor sample, corroborating previous results suggesting that giant planet frequency still is a rising function of host star $[\text{Fe}/\text{H}]$. We also note that all detections in the overall sample are giant long-period planets.

Key words. techniques: radial velocities - methods: data analysis - planetary systems - stars: abundances - stars: individual: HD 220197, HD 233832

* Based on observations made with the HARPS-N spectrograph on the Italian Telescopio Nazionale Galileo (TNG) operated on the island of La Palma (Spain) by the INAF – Fundación Galileo Galilei (Spanish

Osservatorio del Roque de los Muchachos of the Instituto de Astrofísica de Canarias)

1. Introduction

Amongst the physical properties of planet-host stars, mass and metallicity seem to have the biggest impact in promoting the formation of giant ($M > 20 M_{\oplus}$) planets; many studies have long shown that M dwarfs with $M_* < 0.5 M_{\odot}$ are less likely to host a Jupiter-like planet than Sun-like or more massive F and G main-sequence stars (Butler et al. 2004; Johnson et al. 2007, 2010; Bonfils et al. 2013), and that metal-rich stars have a much higher probability to be orbited by at least one giant planet than lower metallicity stars (Gonzalez 1997; Fischer & Valenti 2005; Sozzetti 2004; Santos et al. 2001, 2004; Sozzetti et al. 2009; Mortier et al. 2012).

Of special interest in recent years is the positive correlation between stellar metallicity and occurrence of giant planets, especially since such a correlation is not found between host star metallicity and frequency of sub-Neptunian ($R < 4 R_{\oplus}$, $M \sin i < 10 M_{\oplus}$) planets (Udry et al. 2006; Sousa et al. 2008, 2011; Mayor et al. 2011; Buchhave et al. 2012; Courcol et al. 2016). In particular, Mortier et al. (2012) reports that the fraction of stars hosting a giant planet rises from 5% for solar metallicity values to 25% for metallicities that are twice that of the Sun; these conclusions are also supported by results from the Kepler mission (see e.g. Buchhave et al. 2018).

The correlation between host star metallicity [Fe/H] and frequency of giant planets is usually seen as strong evidence favouring core-accretion over disk instability formation models for giant planets. In the core-accretion model (Pollack et al. 1996; Ida & Lin 2004; Mordasini et al. 2009, 2012) giant planets are formed from the accretion of material into solid cores until they are massive enough ($\sim 10 M_{\oplus}$) to trigger a rapid agglomeration of gas, a process more efficient in metal-rich disks. In the disk instability model (Boss 1997; Mayer et al. 2002; Boss 2002, 2006) giant planets form directly from the collapse of self-gravitating clumps of gas after the disruption of the proto-planetary disk, without requiring the presence of solid cores.

Recent works also show interesting correlations between metallicity regimes and the class of giant planets found around the host star, stressing the importance of stellar metallicity as a proxy for protoplanetary disk chemical composition and its role in driving planet formation and dynamical evolution. Metal-poor stars seem to host planets that are more massive and with longer periods than those hosted by metal-rich stars. Sozzetti (2004) argues for an anti-correlation between orbital period and host star metallicity, a result more recently supported by Mulders et al. (2016) based on an analysis of Kepler candidates; Santos et al. (2017) also report that stars with planets more massive than $4 M_{Jup}$ are on average more metal-poor than stars hosting less massive planets.

Similarly, Maldonado et al. (2015b) report that stars hosting hot Jupiters (defined as giant planets with semimajor axis $a < 0.1$ AU) tend to have slightly higher metallicities than stars orbited by more distant giants, further noticing that no hot Jupiter are found around stars having metallicities lower than -0.6 dex. This result is confirmed by the analysis of 59 cool Jupiter hosts and 29 hot Jupiter hosts in Maldonado et al. (2018), finding a significant deficit of hot Jupiter planet hosts below $+0.2$ dex compared to cool Jupiter planet hosts and interpreting the different chemical characteristics of the host stars of these planetary classes as distinct planetary populations with different evolutionary history; the same study also notes that metal-poor stars hosting cool Jupiters have higher α -element abundances than those hosting hot Jupiters, suggesting that in metal-poor protoplanetary disks an overabundance of elements such as Mg, Si, Ti may

compensate for the lack of Fe in allowing the formation of giant planets according to the core-accretion model. Previous studies (Haywood 2008, 2009; Kang et al. 2011; Adibekyan et al. 2012b,a) had similarly noted that planet-hosting stars having low [Fe/H] tend to be enhanced in α -elements.

Buchhave et al. (2018) also find that stars hosting Jupiter analogues have average metallicities close to that of the Sun, while hot Jupiters as well as cool eccentric ones are found around stars having higher metallicities, suggesting that planet-planet scattering mechanisms producing more eccentric orbits are more common in metallic protoplanetary environments.

The correlation between stellar [Fe/H] and occurrence of giant planets has inspired the search for such planetary bodies around stars specifically selected for their low [Fe/H] values, especially to determine the metallicity limit below which no giant companions are formed. In 2003 a three-years survey using HIRES on the Keck I telescope was started (see Sozzetti et al. 2006, 2009), observing ~ 200 metal-poor ($-2 \leq [\text{Fe}/\text{H}] \leq -0.6$ dex) stars obtaining a $\sim 10 \text{ ms}^{-1}$ Doppler precision and finding no candidate planet. The null detection was therefore used to provide a $1-\sigma$ upper limit of 0.67% for the frequency of massive planets orbiting low-metallicity stars at orbital periods $P < 3$ yr.

Also, one of the High Accuracy Radial velocity Planet Searcher (HARPS, see Mayor et al. 2003) guaranteed time observations (GTO) sub-samples was explicitly build to search for giant planets orbiting metal-poor stars in the southern hemisphere, using the high precision of the spectrograph ($\sim 1 \text{ ms}^{-1}$) to evaluate their frequency and low-metallicity formation limit. The study of this 88 metal-poor stars sub-sample has found a total of three giant planets (HD 171028 b, HD 181720 b, HD 190984 b) having minimum masses of 1.98, 0.37 and $3.1 M_{Jup}$ and orbital periods of 550, 956 and 4885 days, respectively. In addition to these detection, one yet unconfirmed planet was proposed around star HD 107094, having minimum mass of $4.5 M_{Jup}$ and period of 1870 days (see Santos et al. 2007, 2010b, 2011). From these 3 giant planets over 88 target stars, Santos et al. (2011) derive a frequency of Jupiter-mass planets around metal-poor stars of $f_p = 3.4^{+3.2}_{-1.0}\%$, a value that rises to $11.3^{+4.9}_{-5.3}\%$ when considering only the 34 stars in the metallicity range in which the three detected planets have been found and with more than 3 measurements ([Fe/H] between -0.40 and -0.60 dex), and also that the null detection on the 32 sample stars with [Fe/H] < -0.60 dex and at least 6 datapoints implies a frequency of $f_p < 5\%$ for this subsample. All of these results are presented as conservative estimates, due to the possibility of having not detected existing giant companions on short periods due to unoptimal sampling, low number of measurements and considering a possible fourth detection around HD 107094 and several linear trends in the analyzed sample. Interestingly, Santos et al. (2011) further note that the four stars around which the three planets and one candidate were observed have [Fe/H] values (-0.48 , -0.53 , -0.49 and -0.51 dex) on the high-metallicity end of the sample, suggesting that even for metal-poor stars the giant planet frequency is a rising function of the host star metallicity.

A follow-up analysis of the metal-poor samples studied in Sozzetti et al. (2009) and Santos et al. (2011) was presented in Mortier et al. (2012), showing that while no hot Jupiters are found, and are therefore rare around such metal-poor stars ($f_p < 1\%$), the fraction of long-period giant planets is much higher, rising from $f_p < 2.35\%$ at [Fe/H] ≤ -0.7 dex to $f_p = 4.48^{+4.04}_{-1.38}\%$ for stars with [Fe/H] > -0.7 dex.

Furthermore, Johnson & Li (2012) find that the critical value for [Fe/H] under which giant planets are not formed is a function of planetary distance r from the host star, estimating a lower

limit for this value of $[\text{Fe}/\text{H}]_{\text{crit}} \simeq -1.5 + \log r$. Interestingly, claims of giant planets found around exceptionally metal-poor ($[\text{Fe}/\text{H}] \sim -2.0$ dex) stars were disproven by follow-up studies, such as the case of the planetary systems proposed around the stars HIP 11952 (see Desidera et al. 2013; Müller et al. 2013) and HIP 13044 (see Jones & Jenkins 2014). We also note that that, as of the time of writing, the dwarf star with the lowest metallicity known to host any giant planet is HD 155358 with $[\text{Fe}/\text{H}] = -0.62$ dex, hosting two planets with minimum masses of 0.99 and 0.82 M_{Jup} at periods of 194.3 and 391.9 days (see Robertson et al. 2012; Santos et al. 2013)

In this paper we present results from the survey conducted with the High Accuracy Radial velocity Planet Searcher in the Northern hemisphere (HARPS-N, see Cosentino et al. 2012) at the Telescopio Nazionale Galileo (TNG) in La Palma within the observational programme Global Architecture of Planetary Systems (GAPS, see Covino et al. 2013; Desidera et al. 2013) on a northern metal-poor sample. We report the detection of two giant planets around stars HD 220197 and HD 233832 and a preliminary revision of the giant planet frequency f_p . In Sect. 2 we describe the selection and observations conducted with HARPS-N on our northern sample. We characterize the host stars HD 220197 and HD 233832 in Sect. 3 before presenting our orbital solutions in Sect. 4 and the update of planetary frequency in Sect. 5; finally we conclude and discuss the overall results in Sect. 6.

2. The HARPS-N metal-poor sample

The selected stars were drawn from the sample of ~ 200 stars previously observed with Keck/HIRES in a similar search for giant planetary companions around metal-poor ($-2.0 \leq [\text{Fe}/\text{H}] \leq -0.6$ dex) stars (see Sozzetti et al. 2006, 2009) in which the targets selected from the Carney-Latham and Ryan samples of metal-poor, high-velocity field stars (see Carney et al. 1996; Ryan 1989; Ryan & Norris 1991) were surveyed with a $\sim 10 \text{ ms}^{-1}$ precision. A sub-sample of 42 stars was therefore selected for observation with HARPS-N, having metallicity approximately between -1.0 and -0.5 dex, magnitude $V < 11.0$ mag so to allow for photon noise precision of $\sim 1 \text{ ms}^{-1}$ and being chromospherically quiet. The metallicity $[\text{Fe}/\text{H}]$, magnitude V and effective temperature T_{eff} distributions of the sample are shown in Fig. 1.

The 42-stars sample thus selected was monitored with HARPS-N from August 2012 to August 2018, obtaining a total of 1496 datapoints (a mean of 35 observations per star) with a mean error of 1.25 ms^{-1} ; mean exposure time was 800 seconds and mean signal-to-noise ratio (S/N) was 89.30.

The high precision timeseries we obtained were searched for significant (false alarm probability $\text{FAP} \leq 1\%$) signals via a generalized Lomb-Scargle periodogram using the IDL routine GLS (Zechmeister & Kürster 2009); in case of detection of significant signals a single-planet orbital solution is tried out.

Two stars in our sample (HD 220197, HD 233832) show a significant periodogram peak for which a successful search for a planetary solution was made (see Sect. 4) and will therefore be the focus of this work's analysis. The complete list of measurements collected for these two stars is listed in Table 5 at the end of this paper. In Fig. 2 we show as red circles the timeseries of the radial velocities collected for HD 220197 and HD 233832 and activity indexes bisector inverse span (BIS), full width at half maximum (FWHM) of the CCF, $\log R'_{\text{HK}}$, ΔV (see Nardetto et al. 2006) and the new indicator $V_{\text{asy(mod)}}$ defined in Lanza et al. (2018) to avoid the known spurious dependencies with radial velocity variations of the indicator V_{asy} defined in Figueira et al.

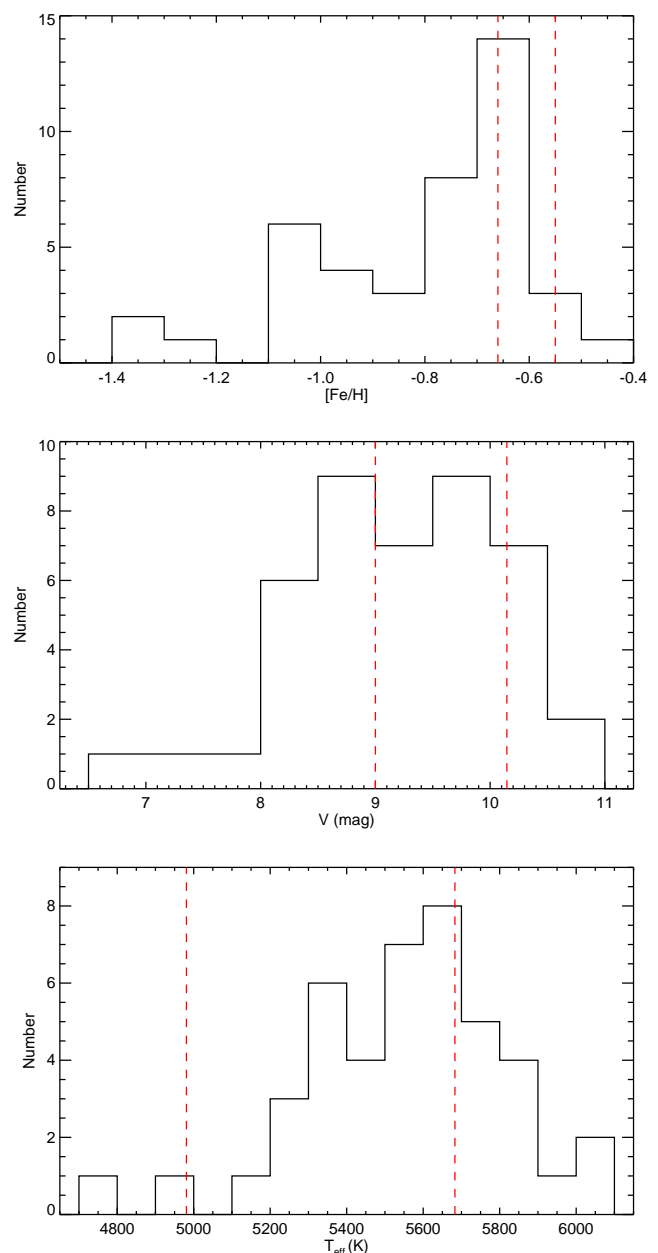


Fig. 1. Metallicity, magnitude and effective temperature distribution of the HARPS-N metal-poor sample discussed in this work. The values of stars HD 220197 and HD 233832 are indicated by the vertical dashed red lines.

(2013) and Figueira et al. (2015). In the FWHM datasets the effect of a defocusing affecting the first portion of the HARPS-N observations is evident as a trend in the datapoints, specifically affecting the first 31 datapoints collected for HD 220197 and the first 11 for HD 233832. This instrumental defocusing was corrected in March 2014 and is absent from the following data. To correct for this defocusing and improve the quality of the collected data by removing spurious correlations between radial velocities and FWHM introduced by this instrumental effect, we follow Benatti et al. (2017) in which the same effect was encountered while characterizing the planetary system orbiting HD 108874 with HARPS-N data within the same time period. After removing two spurious observations at epoch 2456181.62 and 2456602.56 for HD 220197 (see Sect. 4 for details), we per-

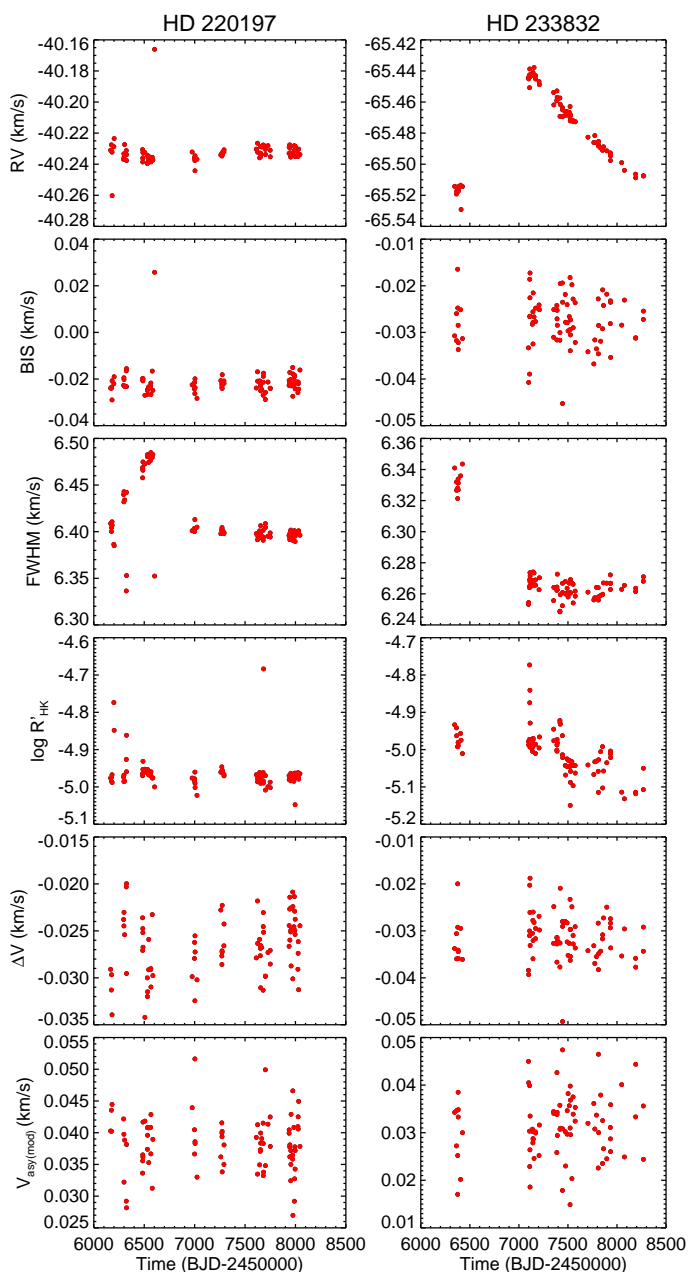


Fig. 2. Timeseries of measurements obtained with HARPS-N on HD 220197 (left column) and HD 233832 (right column). Rows top to bottom show radial velocities, Bisector Inverse Span, CCF FWHM, $\log R'_{\text{HK}}$, ΔV and $V_{\text{asy(mod)}}$ respectively.

formed a polynomial fit on the FWHM data affected by the defocusing and considered the best-fit residuals as corrected FWHM. We report the values of the corrected FWHM in parentheses in the fifth column of Table 5 alongside the uncorrected FWHM values. This correction successfully lowers the correlation between radial velocities and FWHM; for HD 220197 we find a Spearman correlation r between these two quantities of -0.578 before correction and of -0.277 after correction, while for HD 233832 r varies from -0.2466 to 0.008 after correcting for the defocusing. In all following analysis we have used the corrected timeseries.

Table 1. Stellar properties.

Parameter	HD 220197	HD 233832
α (J2000)	$23^{\text{h}}21^{\text{m}}58.2^{\text{s}}$	$11^{\text{h}}26^{\text{m}}05.5^{\text{s}}$
δ (J2000)	$+16^{\circ}37'57''$	$+50^{\circ}22'32''$
π (mas) ^a	15.496 ± 0.046	16.995 ± 0.075
μ_{α} (mas yr ⁻¹) ^a	407.247 ± 0.070	-473.959 ± 0.074
μ_{δ} (mas yr ⁻¹) ^a	-48.264 ± 0.051	124.167 ± 0.087
B (mag) ^b	9.60 ± 0.01	10.92 ± 0.04
V (mag) ^b	9.00 ± 0.01	10.146 ± 0.060
R (mag) ^c	8.764 ± 0.001	9.912 ± 0.001
I (mag) ^c	8.763 ± 0.001	9.047 ± 0.040
G (mag) ^a	8.7448 ± 0.0003	9.899 ± 0.004
J (mag) ^b	7.698 ± 0.020	8.544 ± 0.024
H (mag) ^d	7.362 ± 0.018	8.042 ± 0.061
K (mag) ^b	7.349 ± 0.036	8.013 ± 0.020

Notes. ^(a) retrieved from Gaia Data Release 2 (Brown et al. 2018) ^(b) retrieved from Smart & Nicasro (2014) ^(c) retrieved from Monet et al. (2003) ^(d) retrieved from Cutri et al. (2003)

Table 2. Spectroscopic stellar parameters as obtained using the two different analysis on equivalent width described in Sect. 3

	HD 220197	
T_{eff}	5750 ± 25	5645 ± 19
$\log g$ (cgs)	4.40 ± 0.13	4.42 ± 0.03
ξ (kms ⁻¹)	1.17 ± 0.05	0.91 ± 0.04
[Fe/H]	-0.50 ± 0.09	-0.55 ± 0.02
	HD 233832	
T_{eff}	5075 ± 75	4961 ± 35
$\log g$ (cgs)	4.54 ± 0.15	4.48 ± 0.07
ξ (kms ⁻¹)	1.04 ± 0.02	0.19 ± 0.31
[Fe/H]	-0.54 ± 0.09	-0.67 ± 0.03

3. Stellar properties: HD 220197 and HD 233832

Catalogue stellar parameters for the two host stars are provided in Table 1, while the stellar parameters and elemental abundances obtained from our spectroscopic analysis based on HARPS-N spectra are shown in Table 3.

Effective temperature T_{eff} , surface gravity $\log g$, microturbulence velocity ξ and iron abundance [Fe/H] were measured through equivalent widths and using of a grid of Kurucz model atmospheres (Kurucz 1993) and the spectral analysis package MOOG (Snedden 1973). In particular, T_{eff} was derived by imposing that the Fe I abundance does not depend on the excitation potential of the lines, ξ by imposing that the Fe I abundance is independent on the line equivalent widths, and $\log g$ by the Fe I/Fe II ionization equilibrium condition. To account for possible differences in the calculation of equivalent widths we used two different softwares, namely IRAF (Tody 1993) and ARES2 (Sousa et al. 2015), to compute them from the HARPS-N master spectra for HD 220197 and HD 233832 built from the coaddition of the individual spectra used for the radial velocity measurements. The values of T_{eff} , $\log g$, ξ and [Fe/H] obtained from these two measurements of equivalent widths are respec-

Table 3. Newly derived stellar parameters and elemental abundances. The first errors on elemental abundances refer to the measure of equivalent width, while the errors in parentheses are obtained from the root sum square of the abundance error caused by uncertainties on T_{eff} , $\log g$ and ξ .

Parameter	HD 220197	HD 233832
Mass (M_{\odot}) ^a	0.91 ± 0.02	0.71 ± 0.02
Radius (R_{\odot}) ^a	0.98 ± 0.02	0.68 ± 0.03
Age (Gyr) ^b	10.165 ± 1.367	5.417 ± 4.165
T_{eff} (K) ^c	5683 ± 15	4981 ± 31
$\log g$ (cgs) ^c	4.42 ± 0.03	4.49 ± 0.06
ξ (kms ⁻¹) ^c	1.01 ± 0.03	1.04 ± 0.02
v_{macro} (kms ⁻¹)	3.1	1.8
$v \sin i$ (kms ⁻¹)	1.5 ± 0.5	0.8 ± 0.5
$\log R'_{HK}$	-4.96	-5.01
P_{rot} (d) ^d	~ 19	~ 41
[Fe/H] ^c	$-0.55 \pm 0.02 (+ - 0.06)$	$-0.66 \pm 0.03 (+ - 0.10)$
[C I/H]	$-0.26 \pm 0.09 (+ - 0.04)$	$+0.09 \pm 0.08 (+ - 0.07)$
[Na I/H]	$-0.41 \pm 0.03 (+ - 0.02)$	$-0.60 \pm 0.04 (+ - 0.07)$
[Mg I/H]	$-0.21 \pm 0.04 (+ - 0.02)$	$-0.42 \pm 0.04 (+ - 0.04)$
[Al I/H]	$-0.30 \pm 0.17 (+ - 0.01)$	$-0.46 \pm 0.16 (+ - 0.05)$
[Si I/H]	$-0.35 \pm 0.09 (+ - 0.01)$	$-0.55 \pm 0.08 (+ - 0.03)$
[S I/H]	$-0.27 \pm 0.04 (+ - 0.04)$	$-0.27 \pm 0.09 (+ - 0.07)$
[Ca I/H]	$-0.29 \pm 0.06 (+ - 0.03)$	$-0.51 \pm 0.12 (+ - 0.09)$
[Ti I/H]	$-0.22 \pm 0.06 (+ - 0.03)$	$-0.45 \pm 0.12 (+ - 0.11)$
[Ti II/H]	$-0.40 \pm 0.09 (+ - 0.05)$	$-0.61 \pm 0.09 (+ - 0.06)$
[Cr I/H]	$-0.49 \pm 0.06 (+ - 0.02)$	$-0.65 \pm 0.10 (+ - 0.08)$
[Cr II/H]	$-0.57 \pm 0.06 (+ - 0.05)$	$-0.66 \pm 0.10 (+ - 0.06)$
[Ni I/H]	$-0.51 \pm 0.07 (+ - 0.02)$	$-0.73 \pm 0.09 (+ - 0.04)$
[Zn I/H]	$-0.37 \pm 0.04 (+ - 0.02)$	$-0.61 \pm 0.06 (+ - 0.04)$
[Y II/H]	$-0.66 \pm 0.06 (+ - 0.05)$	$-0.88 \pm 0.10 (+ - 0.06)$
[Zr II/H]	$-0.51 \pm 0.03 (+ - 0.06)$	$-0.59 \pm 0.12 (+ - 0.06)$
[Nd II/H]	$-0.65 \pm 0.08 (+ - 0.06)$	$-0.62 \pm 0.18 (+ - 0.07)$
[Cu I/H]	$-0.52 \pm 0.12 (+ - 0.03)$	$-0.73 \pm 0.16 (+ - 0.05)$
[Eu II/H]	$-0.44 \pm 0.07 (+ - 0.05)$	$-0.47 \pm 0.06 (+ - 0.07)$
[La II/H]	$-0.73 \pm 0.10 (+ - 0.06)$	$-0.82 \pm 0.08 (+ - 0.07)$
[Mn I/H]	$-0.76 \pm 0.09 (+ - 0.03)$	$-0.80 \pm 0.09 (+ - 0.09)$
[Ba II/H]	$-0.73 \pm 0.10 (+ - 0.05)$	$-0.99 \pm 0.09 (+ - 0.05)$

Notes. (a) weighted mean between parameter calculated from PARAM 1.3 (see da Silva et al. 2006) and Yonsei-Yale isochrones (see Yi et al. 2008) (b) calculated from PARAM 1.3 (c) weighted mean between the values obtained from the two analyses on equivalent width described in Sect. 3 (d) calculated following Noyes et al. (1984) and Mamajek & Hillenbrand (2008).

tively shown in the first and second columns of Table 2 and are generally in good agreement; in the following we use the weighted mean of each parameter thus obtained, shown in Table 3. The differential elemental abundances with respect to the Sun were measured from our HARPS-N spectra following the method detailed in Damasso et al. (2015), Biazzo et al. (2015), Santos et al. (2013) and references therein. The first value of uncertainty on elemental abundance is obtained from the measure of the equivalent width, while the second value is the root sum square of the errors on abundance due to the uncertainties in stellar parameters T_{eff} , $\log g$ and ξ .

To compensate between model dependencies, we estimate the stellar mass and radius as the weighted mean of the values obtained from the online tool PARAM 1.3 (see da Silva et al. 2006) and those obtained from the Yonsei-Yale isochrones (see Yi et al. 2008).

It can be noted that the photometric T_{eff} , [Fe/H] and M_{*} reported in Sozzetti et al. (2009) (5564 K, -0.65 dex and $0.83 M_{\odot}$ for HD 220197; 4941 K, -0.74 dex and $0.69 M_{\odot}$ for HD 233832) are lower than the spectroscopic values obtained from HARPS-N, a result already noted in previous works (e.g. Biazzo et al. 2007; Sozzetti et al. 2007; Torres et al. 2012; Tsantaki et al. 2013; Maldonado et al. 2015a).

We synthesize spectral lines around 6200 Å and 6700 Å to obtain an estimate of projected rotational velocity $v \sin i$ from fixed macroturbulence, instrument resolution and limb-darkening coefficient, using the atmospheric models of Kurucz (1993). For HD 220197 assuming from the relations found in Brewer et al. (2016) $v_{macro} = 3.1$ kms⁻¹ we find a projected rotational velocity of $v \sin i = 1.5 \pm 0.5$ kms⁻¹, while for the cooler HD 233832 we assume from the same relations $v_{macro} = 1.8$ kms⁻¹ and obtain a projected rotational velocity of 0.8 ± 0.5 kms⁻¹, below the ~ 2 kms⁻¹ resolution of HARPS-N, suggesting a very slow stellar rotation unless the star is observed nearly pole-on. From this estimates of $v \sin i$ we can give upper limits for the rotational period as $P_{rot} = 2\pi R_{*}/v \sin i$, obtaining values of 31 days for HD 220197 and 43 for HD 233832. Having from our observations mean values of $\log R'_{HK}$ of -4.96 for HD 220197 and -5.01 for HD 233832 (see Sect. 4 and Fig. 2) we can also provide analytical estimates of the rotation period P_{rot} using the empirical relations from Noyes et al. (1984) and Mamajek & Hillenbrand (2008), obtaining values of ~ 19 days and ~ 41 days for HD 220197 and HD 233832 respectively.

We also note that the Second Data Release (DR2) of the astrometric satellite Gaia (see Gaia Collaboration et al. 2016; Brown et al. 2018) has confirmed the existence of a cooler ($T_{eff}=3721^{+230}_{-70}$ K) and fainter ($G=12.71$ mag) stellar companion for HD 233832 at comparable parallax of 17.066 ± 0.053 mas and at 4.8 arcseconds of angular separation, which at a distance of 59 pc (see Table 1 for the parallax value of the star) implies a projected separation of 280 AU. This stellar object was listed as a possible companion for HD 233832 in previous catalogs (e.g. Cutri et al. 2003) but in the absence of measurements of parallax its was not possible to confirm its binarity nature before the release of Gaia DR2 astrometry measurements. Assuming a metallicity value similar to that of the primary star we use the Yonsei-Yale isochrones to provide a first estimate of mass and radius for this companion star respectively of $0.420 \pm 0.049 M_{\odot}$ and $0.367 \pm 0.026 R_{\odot}$. Having therefore an estimate of the mass and orbital projected separation of both stellar components, we can give a first assessment of the order of magnitude of the stellar companion's orbital period as $P_B \sim 4400$ yr.

The results on elemental abundances allow us to investigate to which population the two targets belong. We thus considered the abundances of field stars listed in the catalogs by Soubiran & Girard (2005) and Adibekyan et al. (2012c) and applied the prescriptions reported in Biazzo et al. (2015). We thus used as abundance of α -elements that obtained from magnesium, silicon, calcium, and titanium. Fig. 3 shows the position of HD 220197 and HD 233832 in the $[\alpha/Fe]$ versus [Fe/H] diagram. Based on these chemical indicators, the star HD 220197 seems to be more likely a thick-disk star than HD 233832, the latter lying in a metallicity region populated by both thin and thick-disk stars.

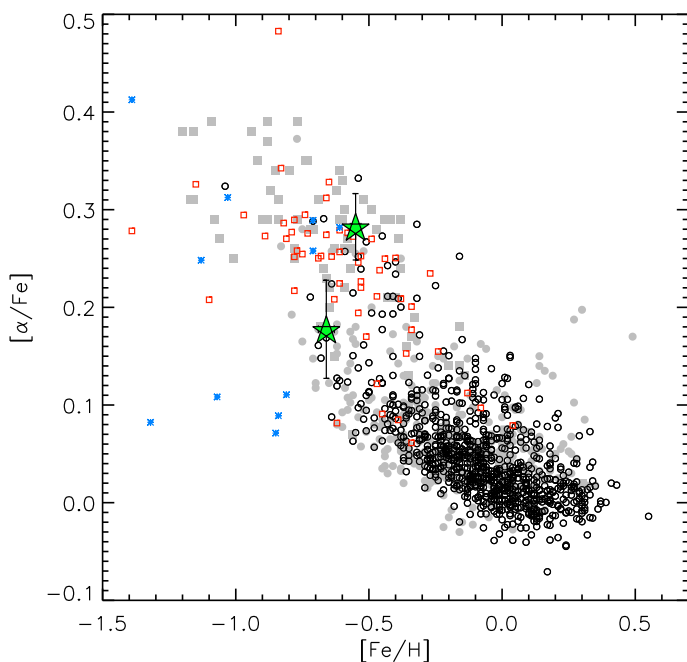


Fig. 3. $[\alpha/\text{Fe}]$ versus $[\text{Fe}/\text{H}]$ for HD 220197 (upper star symbol) and HD 233832 (lower star symbol). Thin-disk, thick-disk, and halo stars are shown with circles, squares, and asterisks, respectively (filled symbols: Soubiran & Girard (2005); open symbols: Adibekyan et al. (2012c)).

Another way to classify the two stars as either thin- or thick-disk objects is to use statistical indicators purely based on kinematics, that can then be compared with our inference based on the chemical indicator $[\alpha/\text{Fe}]$. In order to calculate the likelihood of any given object belonging to either of the two populations on the basis of its Galactic kinematics, a number of approaches can be adopted. We elect to carry out population assignments using the classifications by Bensby et al. (2003, 2005). First, we combine systemic radial velocity and Gaia DR2 proper motion and parallax for both stars to calculate the Galactic velocity vector (U, V, W , with U positive toward the Galactic anticenter) with respect to the local standard of rest (LSR), adjusting for the standard solar motion $(U_{\odot}, V_{\odot}, W_{\odot}) = (-8.5, 13.38, +6.49)$ kms^{-1} (following Coskunoglu et al. 2011). Then, we calculate the thick disc-to-thin disk probability ratio TD/D using the prescriptions of Bensby et al. (2003, 2005) for the velocity dispersion and asymmetric drift of the assumed Gaussian velocity ellipsoid for the two populations, and the observed fractions of each population in the solar neighborhood (4% and 96%, respectively). Bensby et al. (2003) suggest as threshold to clearly identify thick- and thin-disk stars values of $TD/D \geq 10$ and $TD/D \leq 0.1$, respectively. Finding for HD 233832 and HD 220197 $TD/D = 1113$ and $TD/D = 2.8$, respectively, HD 233832 is rather clearly a thick-disk object, while for HD 220197 the evidence is for an object with kinematics intermediate between that of thin and thick disk.

Using the results from both methods, we can therefore reasonably classify both HD 220197 and HD 233832 as thick-disk object within the uncertainties of the disk populations.

4. Radial velocity analysis

Having found significant peaks in the radial velocities periodograms for stars HD 220197 and HD 233832, we searched for a single-planet orbital solution via a differential evolution Markov chain Monte Carlo method (Eastman et al. 2013;

Desidera et al. 2014), the nine free parameters being inferior conjunction epoch T_c , orbital period P , $\sqrt{e} \cos \omega$, $\sqrt{e} \sin \omega$, semi-amplitude K , and a zero-point radial velocity γ and an uncorrelated jitter term j for each instrument (Keck and HARPS-N). Uninformative priors were used for all parameters. Eighteen chains were run simultaneously and reached convergence and good mixing according to the criteria established in (Eastman et al. 2013).

To ensure that the detected signals are not of stellar origin we search for correlations between radial velocities and activity indexes bisector inverse span (BIS), full width at half maximum (FWHM) of the CCF, $\log R'_{\text{HK}}$, ΔV and $V_{\text{asy(mod)}}$. To obtain values of BIS, FWHM, ΔV and $V_{\text{asy(mod)}}$ from our HARPS-N spectra we use the IDL procedure presented in Lanza et al. (2018), while $\log R'_{\text{HK}}$ is obtained as detailed in Lovis et al. (2011).

The fitted and derived parameters and their 1σ uncertainties, taken as the medians of the posterior distributions and their 34.13% intervals, are listed in Table 4 and discussed in the following paragraphs.

HD 220197 We observed this star with HARPS-N from August 2012 to October 2017, obtaining 88 measurements with mean S/N of ~ 110 that we join with the 5 Keck datapoints from Sozzetti et al. (2009); we note that the seven HARPS-N spectra obtained between epochs 2456166.69 and 2456201.60 were taken with only the spectral orders falling on the blue side of the CCD. From these datapoints we exclude the one taken at epoch 2456181.62 due to low S/N and the one taken at epoch 2456602.56, which shows highly discrepant values in radial velocity, BIS and FWHM compared to the mean values of the time-series (see Fig. 2 and Table 5) and therefore suggesting that this particular observation is affected by an instrumental effect that we are not able to completely correct.

The periodogram of the timeseries (see top panel of Fig. 5) shows a highly significant peak at ~ 1720 days with a false alarm probability of 0.01% as calculated via bootstrap method which appears to be uncorrelated with any of the activity indexes analyzed (see bottom panels of Fig. 5) and therefore not of clear stellar origin. The data is best fitted by a Keplerian curve (see Fig. 4 and first column of Table 4) having semiamplitude $K=3.78^{+1.78}_{-0.72}$ ms^{-1} , period $P=1728^{+162}_{-80}$ days and eccentricity $e=0.187^{+0.279}_{-0.132}$, from which we obtain a planetary minimum mass of $0.20^{+0.07}_{-0.04} M_{\text{Jup}}$ and semimajor axis of $2.729^{+0.168}_{-0.085}$ AU.

To account for any offset or inconsistency between the half-chip and full-chip data we also search for an orbital solution treating the two groups of data as independent datasets allowing for an offset between them. The resulting solution features a Bayesian Information Criterion value (BIC) of 326.62, similar to the BIC value of 321.69 obtained for the solution lacking any distinction between full-chip and half-chip data shown in Fig. 4 and Table 4. The introduction on an offset between half-chip and full-chip data is not clearly statistically preferred and we therefore find no compelling reason to treat them as independent datasets. A similar case is represented by Desidera et al. (2013), in which the inclusion or lack of an offset between half-chip and full-chip data collected with HARPS-N also turned out to be non significant in the analysis of the radial velocity data of the metal-poor star HIP 11952.

While a low-power peak can be found in both FWHM and $\log R'_{\text{HK}}$ periodograms (see fourth and fifth panels of Fig. 5) near the proposed orbital period for HD 220197 b, we stress that both are non-significant peaks, having a FAP of 100% and 99.4% respectively.

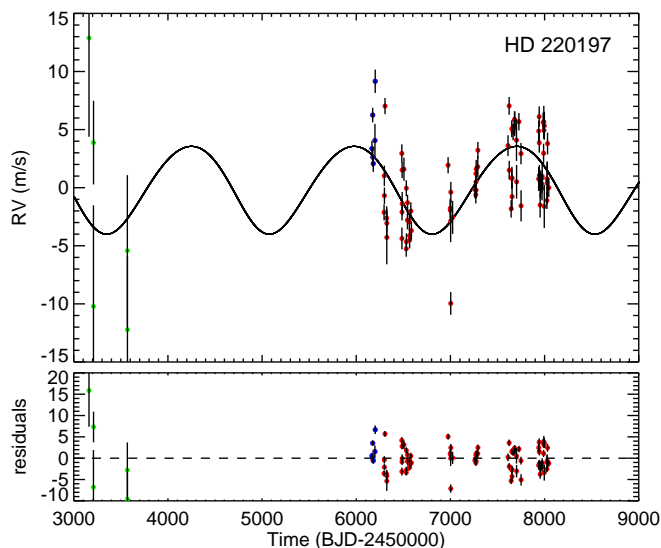


Fig. 4. Orbital fit for the planet HD 220197 b. In the top panel, our best-fit solution is shown as a black curve over the literature datapoints from Keck (green) and our HARPS-N observations (blue for blue-chip data, red for full-chip data). The bottom panel shows the residual radial velocities.

The post-fit residual data show a maximum peak around a period of ~ 17 days, near our expected stellar rotation period of 19 days (see Sect. 3), and another peak of comparable power at ~ 80 days; both peaks have an associated FAP of 55% and are therefore non-significant (see second panel of Fig. 5).

HD 233832 We monitored this star with HARPS-N from February 2013 to May 2018, obtaining 80 HARPS-N measurements with mean S/N of ~ 74 ; an additional 5 Keck datapoints were collected from Sozzetti et al. (2009).

The HARPS-N data clearly show a $\sim 80 \text{ ms}^{-1}$ variation in radial velocities, although we note that our observations failed to satisfactorily sample the minimum and rising portions of this variation. It may be argued that such a variation in radial velocity could be related to the stellar companion recently confirmed by Gaia at angular separation of 4.8 arcseconds and for which we provide a first estimate of $M_B = 0.420 \pm 0.049 M_\odot$ and $R_B = 0.367 \pm 0.026 R_\odot$ (see Sect. 3). We however propose that this is not the case; following the example set in Torres (1999) we can estimate the acceleration $d(RV)/dt$ caused by the stellar companion on the primary as:

$$\frac{d(RV)}{dt} = G \frac{M_B}{a^2(1-e)} \frac{(1 + \cos v) \sin(v + \omega) \sin i}{(1 + \cos E)(1 - e \cos E)} \quad (1)$$

being $a = a_A(M_A + M_B)/M_B$ the semimajor axis of the relative orbit, v the true anomaly, i the mutual inclination and E the eccentric anomaly. Having no estimate on the orbital elements of the companion star except for the projected separation ~ 280 AU, we generated 10^5 possible combinations of orbital elements (e, v, ω, E, i) from which we obtain a mean acceleration of $0.39 \text{ ms}^{-1}\text{yr}^{-1}$; in addition to this we estimate the maximum acceleration for a circular, edge-on stellar orbit to be $0.14 \text{ ms}^{-1}\text{yr}^{-1}$. Both values, we note, are exceptionally low and would cause a variation of at most $\sim 5.82 \text{ ms}^{-1}$ over our 15 years baseline. We therefore argue that the origin of the observed $\sim 80 \text{ ms}^{-1}$ variation in the radial velocities of HD 233832 is not the gravitational influence of its long-period stellar companion.

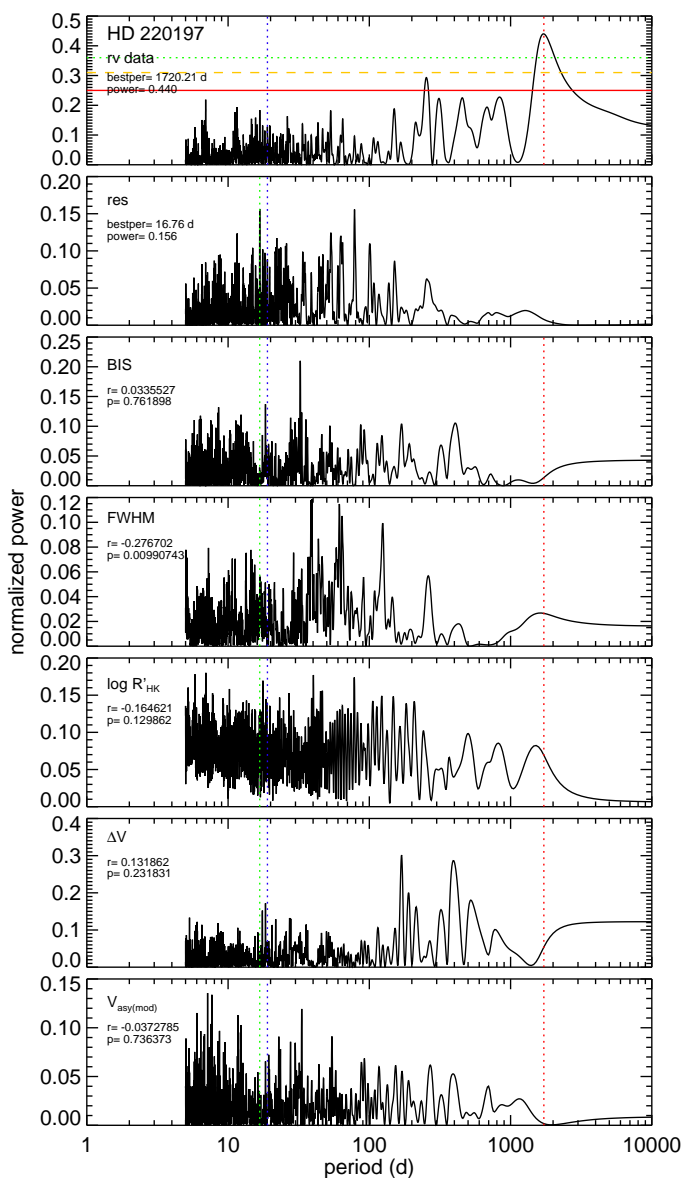


Fig. 5. Activity indexes periodograms for the star HD 220197. The two top panels show the periodograms for the radial velocity data and post-fit residuals; the most significant period value and power are shown in the upper right corner, while the horizontal lines indicate the false alarm probability levels of 10% (solid red), 1% (dashed orange) and 0.1% (dotted green). The following lower panels show the periodograms for bisector inverse span, FWHM, $\log R'_{\text{HK}}$, ΔV and $V_{\text{asy(mod)}}$ with Spearman correlation rank r and significance p with radial velocity data shown in each panel. The most significant periods for radial velocity data and residuals are highlighted in all panels respectively as a red and green vertical dotted line, while the star's rotation period is indicated by a blue vertical dotted line.

The radial velocities periodogram (see top panel of Fig. 7) shows a region of significant power between 1000 and 6000 days, peaking around 1920 days with a FAP of 0.01%. The MCMC we launched with uniform priors returned a Keplerian best-fit with orbital period $P = 2106^{+813}_{-57}$ days showing a large upper error bar; this solution also has a period posterior distribution featuring two peaks of comparable likelihood around $P \sim 2000$ d and $P \sim 4000$ d. To try and solve this apparent degeneracy in period, we fit again the data setting Gaussian priors on the orbital period centered on 2000 and 4000 days with width of 500 days

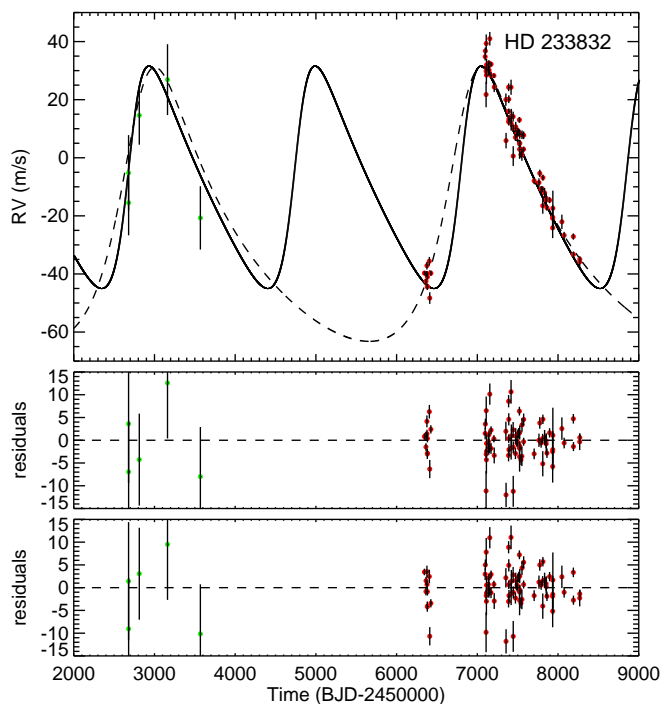


Fig. 6. Same as Fig. 4 but for the planet HD 233832 b. Literature Keck datapoints are shown in green and our HARPS-N data are in red. The solid black curve shows the solution obtained setting prior on orbital period centered on 2000 days, while the dashed curve is derived from orbital prior centered around 4000 days. The second and third panels show respectively the residuals from the 2000 and 4000 days solutions.

in order to determine which period is statistically favourite; a comparison between the results of these fits is shown in Fig. 6 and Table 4.

We thus find two solutions mainly distinguished by their values in semi-amplitude, period and minimum planetary mass. Choosing a prior centered around 2000 days returns a Keplerian solution having $K=38.29^{+2.08}_{-1.35}$ ms^{-1} , $P=2058^{+47}_{-40}$ days and $M\sin i = 1.78^{+0.08}_{-0.06}$ M_{Jup} , while the prior around 4000 days returns a solution having $K=47.18^{+3.63}_{-3.21}$ ms^{-1} , $P=4047^{+91}_{-117}$ days and $M\sin i = 2.72^{+0.23}_{-0.23}$ M_{Jup} . It is clearly seen by comparing the Bayesian Information Criterion value for each solution (of 355.02 and 357.16 respectively) that none is strongly preferred above the other, although the $P \sim 2000$ d solution is formally preferred for having a slightly lower BIC value; no solid conclusion on the value of the planet's orbital period is therefore possible with the available data.

While the presence of the giant planet is clear, the values of its orbital period and mass remain ambiguous and more data with better sampling of the radial velocity minimum and its rise to maximum are needed to discriminate between the two solutions. Another way to resolve this ambiguity may come from observations with the astrometric satellite Gaia, which by the end of its five-years mission will have observed a significant portion of both proposed orbits. We can calculate the astrometric signatures produced on the host star by these two possible solutions as:

$$\alpha = \frac{M_p a}{M_* d} \quad (2)$$

where α is in arcseconds, if planetary and stellar mass are given in solar mass units, semimajor axis a in AU and stellar distance d in parsec. We then find $\alpha \sim 115 \mu\text{as}$ for the $P \sim 2000$ d solution

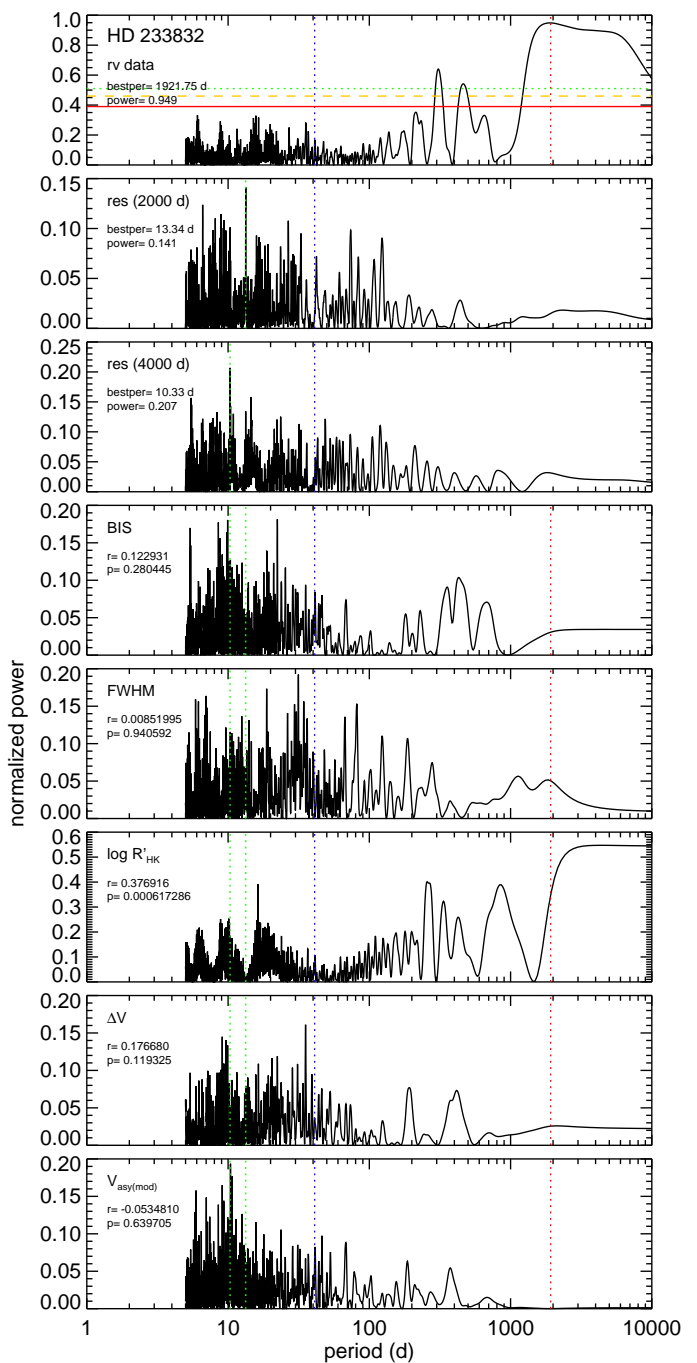


Fig. 7. Same as Fig. 5 but for the star HD 233832.

and $\alpha \sim 278 \mu\text{as}$ for the $P \sim 4000$ d solution, both expected to be detected at high S/N by Gaia for a star this bright ($G = 9.899$ mag).

The periodograms on residual data for the two different orbital solutions (see the second and third panels of Fig. 7) show major peaks at around 13 days for the $P \sim 2000$ d solution and around 10 days for the $P \sim 4000$ d solution with associated FAP of 27% and 52% respectively and therefore both non-significant.

We also find in the periodogram of activity index $\log R'_{\text{HK}}$ a clue of an uncorrelated long-period activity trend in the same period range of our proposed planetary solutions (see sixth panel of Fig. 7). While the blending of the target star spectra with a nearby star can produce similar effects in the activity indexes (see Santos et al. 2002), the known star nearest to HD 233832

Table 4. Orbital fit results

Parameter	HD 220197 b		HD 233832 b			
			(prior P~2000 d)		(prior P~4000 d)	
K (ms ⁻¹)	3.78 ^{+1.78} _{-0.72}		38.29 ^{+2.08} _{-1.35}		47.18 ^{+3.63} _{-3.21}	
P (days)	1728 ⁺¹⁶² ₋₈₀		2058 ⁺⁴⁷ ₋₄₀		4047 ⁺⁹¹ ₋₁₁₇	
$\sqrt{e} \cos \omega$	-0.227 ^{+0.358} _{-0.386}		0.143 ^{+0.074} _{-0.069}		0.481 ^{+0.055} _{-0.075}	
$\sqrt{e} \sin \omega$	0.127 ^{+0.237} _{-0.251}		-0.577 ^{+0.042} _{-0.044}		-0.384 ^{+0.046} _{-0.058}	
T_c	2456416.9 ^{+138.3} _{-83.2}		2457688.8 ^{+27.6} _{-32.5}		2457854.6 ^{+52.8} _{-52.8}	
e	0.187 ^{+0.279} _{-0.132}		0.359 ^{+0.046} _{-0.039}		0.381 ^{+0.029} _{-0.028}	
ω (deg)	159.011 ^{+54.933} _{-80.914}		283.903 ^{+7.543} _{-6.901}		321.365 ^{+6.230} _{-8.792}	
M sin i (M_J)	0.20 ^{+0.07} _{-0.04}		1.78 ^{+0.08} _{-0.06}		2.72 ^{+0.23} _{-0.23}	
a (AU)	2.729 ^{+0.168} _{-0.085}		2.827 ^{+0.045} _{-0.039}		4.438 ^{+0.070} _{-0.090}	
T_{peri} (days)	2456636.3 ^{+196.1} _{-428.0}		2456815.8 ^{+82.6} _{-88.0}		2456874.9 ^{+75.4} _{-89.9}	
	γ	jitter	γ	jitter	γ	jitter
	(ms ⁻¹)	(ms ⁻¹)	(ms ⁻¹)	(ms ⁻¹)	(ms ⁻¹)	(ms ⁻¹)
Keck	2.22 ^{+5.50} _{-6.05}	9.57 ^{+9.65} _{-5.57}	-16.23 ^{+10.64} _{-9.80}	10.55 ^{+17.12} _{-7.59}	-38.78 ^{+13.03} _{-10.10}	10.28 ^{+17.31} _{-7.38}
HARPS-N	-0.92 ^{+0.44} _{-0.58}	2.62 ^{+0.25} _{-0.22}	-7.29 ^{+3.53} _{-3.03}	3.18 ^{+0.38} _{-0.33}	-28.84 ^{+1.88} _{-1.82}	3.35 ^{+0.39} _{-0.35}
BIC	321.69		355.02		357.16	

is its companion confirmed by Gaia observations at 4.8 arcseconds, an angular distance much higher than the 1 arcsecond aperture on the sky of HARPS-N fibers and therefore unlikely to cause such an effect. While it may also be argued that such an activity trend may in fact produce the observed radial velocity variation of HD 233832 and therefore mimic the presence of a massive planet, it is worthy of note that most cases of activity-induced radial velocity signals mimicking giant planets have semiamplitudes of 10 ms⁻¹ or less (see Endl et al. 2016; Johnson et al. 2016; Carolo et al. 2014, for recent examples), much lower than the ~40 ms⁻¹ semiamplitude observed in our HARPS-N data; the 11-year activity cycle of the Sun itself produces a radial velocity variation of 4.98 ± 1.44 ms⁻¹, as detailed in Lanza et al. (2016). Also, the analysis on 304 FGK stars reported in Lovis et al. (2011) and conducted with HARPS concludes that while 61% of old solar-type stars have a detectable activity cycle inducing long-period radial velocity signals, the semiamplitude of the effect is limited in the worst case of their sample to ~11 ms⁻¹ and more typical values are usually less than 3 ms⁻¹.

To further support this point, we can give an estimate of the radial velocity perturbation caused by different activity effects related to stellar rotation using the relations found in Saar & Donahue (1997); Saar et al. (1998); Saar & Fischer (2000) between projected rotational velocity $v \sin i$, macroturbulent velocity v_{macro} and percentage of surface area covered by spot distribution inhomogeneity f_s (ranging from zero for old, inactive stars to several percent for active stars); we also note that Saar et al. (1998) derives that old, slow-rotating stars ($v \sin i \leq 2$ kms⁻¹, $P_{rot} \geq 15$ d) generally have very low mean activity-related radial velocity noise ($\langle \sigma'_v \rangle \sim 4.6$ ms⁻¹). From spectroscopic analysis (see Sect. 3 and Table 3) we have found for HD 233832 a projected velocity of $v \sin i = 0.8$ kms⁻¹ assuming $v_{macro} = 1.8$ kms⁻¹; using as suggested in Saar & Donahue (1997) the relation $f_s \sim 0.4 \Delta y$ being the Strömgren index $\Delta y = 0.518 \pm 0.008$ mag for HD 233832 (see Mints & Hekker 2017) we obtain $f_s \sim 0.21\%$. We therefore find a spot-related perturbation $A_s = 1.26$ ms⁻¹, a bisector velocity span variation

$A_c = 0.013$ ms⁻¹ and a weighted velocity dispersion $\sigma'_v = 3.39$ ms⁻¹, all well below our observed ~80 ms⁻¹ variation.

To also account for radial velocity variations induced by long-term magnetic activity cycles (see Santos et al. 2010a; Lovis et al. 2011; Dumusque et al. 2011) that may mimic the presence of a long-period giant planet we instead use the empirical models found in Lovis et al. (2011) providing a relationship between effective temperature, metallicity and the measured $\log R'_{HK}$ semiamplitude. The latter being 0.055 for our observations of HD 233832 (see bottom right panel of Fig. 2) we then find an estimate of the radial velocity semiamplitude induced by the stellar magnetic activity cycle of $A_{RV} \sim 0.30$ ms⁻¹, also much lower than the observed radial velocity variation of HD 233832.

While caution is certainly needed in announcing the existence of exoplanets, we propose that the signals found in the radial velocity timeseries of stars HD 220197 and HD 233832 are best explained by the existence of the giant planets described in the previous paragraphs.

Due to its low semiamplitude of ~4 ms⁻¹, the signal found in the data collected for star HD 220197 would clearly benefit from further observation and analysis; however we find this signal to be uncorrelated with any significant stellar activity indexes and that a planetary origin remains the most likely explanation given the analysis at hand.

Considering instead HD 233832, while we cannot completely rule out the presence of a magnetic activity cycle at about either 2000 or 4000 days, we argue that a planetary origin for the radial velocity signal observed for HD 233832 seems to be more likely than one exclusively induced by stellar activity since the amplitude of activity-induced radial velocity variations are proven to be much lower than the one we observe. The possibility of a long-term activity cycle for the star HD 233832 having a similar period to the orbital period of planet b still remains, a situation similar to the ~11 years period of both Jupiter and the magnetic cycle of the Sun in the Solar System that deserves future investigation.

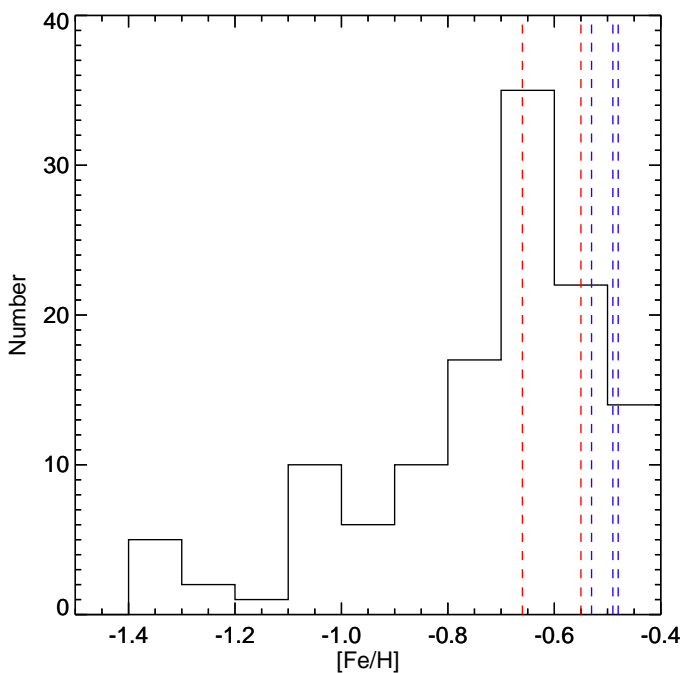


Fig. 8. Metallicity distribution for the 130 metal-poor stars, distributed in the two hemispheres. The metallicities of stars HD 220197 and HD 233832 are indicated by the vertical dashed red lines, while the metallicities of southern host stars HD 171028, HD 181720 and 190984 are shown as blue dashed lines (see Santos et al. 2011).

5. Planetary frequency

Joining the two detections over our 42-stars northern sample with the three detections and one candidate in the 88-stars southern sample analysed in Santos et al. (2007, 2010b, 2011), we obtain a total of five detected giant planets (HD 171028 b, HD 181720 b, HD 190984 b, HD 220197 b and HD 233832 b) and one candidate (around HD 107094) over 130 metal-poor stars. In Fig. 8 the metallicity distribution of the overall sample is shown (values from Santos et al. (2011) for the southern sample and from Sozzetti et al. (2009) for the northern sample), and it can be noted that all detected planets are found in stars in the metal-rich end of the sample; the same applies to the candidate around HD 107094 having a stellar $[\text{Fe}/\text{H}] = -0.51$ dex. We also note that the planets HD 220197 b and HD 233832 b presented in this work orbit the lowest metallicity stars around which detected planets are found in the combined HARPS+HARPS-N sample.

While an accurate estimate of the frequency f_p of giant planets around metal-poor stars would require an assessment of the survey detection limits and will be the subject of a future paper, we can preliminarily note that the 5 detected planets all have high radial velocity semi-amplitude, ranging from the $K \sim 4 \text{ ms}^{-1}$ signal of HD 220197 b to the $K \sim 60 \text{ ms}^{-1}$ signal of HD 171028 b; the same also applies to the proposed $K \sim 88 \text{ ms}^{-1}$ planetary signal for the star HD 107094 (see Santos et al. 2011). The orbital periods are also long, ranging from the $P \sim 550$ d of HD 171028 b to the $P \sim 4885$ d of HD 190984 b. We can therefore assume that such combinations of high-value semi-amplitude and periods would be detectable 100% of the times with the high-precision of HARPS and HARPS-N, with the possible exception of HD 220197 b having the lowest K of all detected signals.

We can therefore provide a preliminar estimate of the occurrence frequency of giant planets in our metal-poor sample f_p

using the binomial distribution:

$$p(m; N, f_p) = \frac{N!}{m!(N-m)!} f_p^m (1-f_p)^{N-m} \quad (3)$$

being $N = 130$ our whole two-hemisphere sample assuming a detection completeness for the semi-amplitudes and periods of our planetary signals and m the number of detections in the sample. By considering only the 5 detected giant planets we thus obtain a frequency of $f_p = 3.84^{+2.45}_{-1.06}\%$, while by including also the candidate signal found for star HD 107094 we have $m = 6$ and a frequency $f_p = 4.61^{+2.58}_{-1.21}\%$, the uncertainty in both values being the $1-\sigma$ error bar. We note that both frequency values are compatible and slightly better constrained than the $3.4^{+3.2}_{-1.0}\%$ value obtained by Santos et al. (2011) for their three detections in the 88-stars southern sample.

We stress that the detected planets all lie in the metal-rich end of the two-hemisphere sample, ranging from $[\text{Fe}/\text{H}] \sim -0.7$ dex to -0.4 dex. Considering only the 67 stars in this metallicity range, we obtain a frequency of $f_p = 7.46^{+4.53}_{-2.07}\%$, comparable with the $\sim 5\%$ estimate for $[\text{Fe}/\text{H}] \sim 0$ dex obtained by Mortier et al. (2012), Mortier et al. (2013) and Gonzalez (2014). If we instead consider the 63 stars in the metal-poor end of the sample ($[\text{Fe}/\text{H}] < -0.7$ dex) in which no giant planets were found in the two-hemisphere sample, we obtain an upper limit on frequency of $f_p < 1.76\%$, significantly lower than the other values obtained by our analysis again showing f_p to be a rising function of $[\text{Fe}/\text{H}]$ even at this low metallicity values.

6. Summary and discussion

In this work we report the detection of the two long-period giant planets HD 220197 b and HD 233832 b as a result of the intense observation of 42 metal-poor stars with HARPS-N conducted as a complement to the study of the southern metal-poor sample previously detailed in Santos et al. (2007, 2010b, 2011) and to continue the analysis of the correlation between stellar metallicity and giant planet frequency (Gonzalez 1997; Sozzetti 2004; Sozzetti et al. 2009; Mortier et al. 2012; Santos et al. 2011). This correlation is usually proposed as strong evidence in favour of core-accretion formation for giant planets over disk instability processes.

We have characterized in Sect. 3 the host stars as α -enriched stars likely members of the thick-disk stellar population; this agrees with previous studies (Adibekyan et al. 2012b,a) finding that metal-poor host stars tend to have a significant overabundance of α -elements and be part of the thick-disk population compared to non-hosting stars; in addition Maldonado et al. (2018) also notes that stars hosting cool Jupiters like HD 220197 b and HD 233832 b also have higher α abundances than stars hosting hot Jupiters, suggesting that the low $[\text{Fe}/\text{H}]$ content in such protoplanetary disks may be compensated by this overabundance of α -elements allowing the formation of planetary cores.

We find HD 220197 b to be characterized as a $M \sin i = 0.20^{+0.07}_{-0.04} M_J$ orbiting its host star with a period of 1728^{+162}_{-80} days; although it could be noted that this low-amplitude signal ($K = 3.78^{+1.78}_{-0.72} \text{ ms}^{-1}$) should be treated with caution, we find that given the results of the current analysis the planetary nature of the signal remains the most likely explanation. We note that this planet is the least massive long-period ($P > 1$ yr) giant planet found around such a metal-poor star, an interesting counter-example to the tendency of metal-poor stars to host more massive planets (e.g. Santos et al. 2017).

On the other hand, the orbital characteristics of HD 233832 are more ambiguous, finding two solutions of equal statistical weight at $P=2058_{-40}^{+47}$ d and $P=4047_{-117}^{+91}$, returning possible minimum masses of $1.78_{-0.06}^{+0.08} M_J$ and $2.72_{-0.23}^{+0.23} M_J$, clearly needing more radial velocity data providing a better sampling of its Doppler variation to discriminate between the two competing solutions. Since the analysis of stellar activity is always an important part in searching for planetary signals, extra special care was taken in handling the signal found for HD 233832 due to the presence of a long-period activity signal in the periodogram of activity index $\log R'_{HK}$ near our proposed orbital solutions. Following the analysis of activity-induced radial velocity signals of Saar & Donahue (1997); Saar et al. (1998); Saar & Fischer (2000); Santos et al. (2010a); Lovis et al. (2011); Dumusque et al. (2011) we argue however that such activity signals would be at most of the order of 5 ms^{-1} , well below the $\sim 80 \text{ ms}^{-1}$ variation observed for HD 233832, suggesting a planetary origin for the radial velocity signal. The same applies for the influence of its stellar companion at angular separation of 4.8 arcseconds recently detected by Gaia. Not being however able to completely rule out the presence of a low-amplitude activity cycle having period similar to our solutions for HD 233832 b, similarly to what is found in the Solar System for the orbital period of Jupiter and the magnetic activity cycle of the Sun, more analysis will be needed to fully characterize this interesting planetary system.

Joining our detections with the three giant planets (HD 171028 b, HD 181720 b and HD 190984 b) detected in the HARPS metal-poor sample (see Santos et al. 2011) we obtain a total of five detections over 130 metal-poor stars. In a preliminary statistical analysis, assuming survey completeness for the high-value radial velocity semiamplitudes (4 to 60 ms^{-1}) and periods (550 to 4885 days) of the detected planets, we find a frequency of giant planets around metal-poor stars of $3.84_{-1.06}^{+2.45}\%$; this value rises to $4.61_{-1.21}^{+2.58}\%$ when including also the candidate planetary signal found in the southern sample around HD 107094 (see Santos et al. 2011). If we instead consider only the 67 stars in the metallicity range ($-0.7 < [\text{Fe}/\text{H}] < -0.4$ dex) in which the detected planets are found, the frequency rises to $f_p = 7.46_{-2.07}^{+4.53}\%$, a value similar to literature estimates on giant planets frequency around solar-metallicity stars (see Mortier et al. 2012, 2013; Gonzalez 2014). We stress that, similarly to the case of the Santos et al. (2011) analysis, our frequency results are conservative as we do not account for completeness in the survey, which will be the subject of a future paper.

Interestingly, the host stars lie in the metal-rich end of the overall stellar sample, reinforcing previous results suggesting that frequency of giant planets continues to be a rising function of stellar metallicity even for metal-poor stars and favouring core-accretion processes for the formation of giant planets (Ida & Lin 2004; Mordasini et al. 2009); this is also reinforced by the $f_p < 1.76\%$ obtained from the null detections below $[\text{Fe}/\text{H}] < -0.7$ dex. We however note that our calculation of f_p should be seen as a preliminary update of giant planets frequency around metal-poor stars, and that a more rigorous assessment of its value will be the subject of a future paper.

While the correlation between stellar metallicity and occurrence of giant planets continues to be confirmed by observations, more analysis is clearly needed to provide a more solid observational basis on which to shed light on planet formation mechanisms and their relation to host star characteristics.

Acknowledgements. We thank the anonymous referee for the useful comments. The GAPS project acknowledges the support by INAF/Frontiera through the

"Progetti Premiali" funding scheme of the Italian Ministry of Education, University, and Research. DB acknowledges financial support from INAF and Agenzia Spaziale Italiana (ASI grant n. 014-025-R.1.2015) for the 2016 PhD fellowship programme of INAF. NCS and JF acknowledge the support by the Fundação para a Ciência e Tecnologia (FCT) through national funds and by FEDER through COMPETE2020 by grants UID/FIS/04434/2013 & POCI-01-0145-FEDER-007672. This work was also funded by FEDER - Fundo Europeu de Desenvolvimento Regional funds through the COMPETE 2020 - Programa Operacional Competitividade e Internacionalização (POCI), and by Portuguese funds through FCT in the framework of the project POCI-01-0145-FEDER-028953 and POCI-01-0145-FEDER-032113. L.M. acknowledges support from the Italian Minister of Instruction, University and Research (MIUR) through FFABR 2017 fund. L.M. also acknowledges support from the University of Rome Tor Vergata through "Mission: Sustainability 2016" fund. G.S. acknowledges financial support from "Accordo ASI-INAF" No. 2013-016-R.0 July 9, 2013 and July 9, 2015.

References

- Adibekyan, V. Z., Delgado Mena, E., Sousa, S. G., et al. 2012a, *A&A*, 547, A36
 Adibekyan, V. Z., Santos, N. C., Sousa, S. G., et al. 2012b, *A&A*, 543, A89
 Adibekyan, V. Z., Sousa, S. G., Santos, N. C., et al. 2012c, *A&A*, 545, A32
 Benatti, S., Desidera, S., Damasso, M., et al. 2017, *A&A*, 599, A90
 Bensch, T., Feltzing, S., & Lundström, I. 2003, *A&A*, 410, 527
 Bensch, T., Feltzing, S., Lundström, I., & Ilyin, I. 2005, *A&A*, 433, 185
 Biazzo, K., Gratton, R., Desidera, S., et al. 2015, *A&A*, 583
 Biazzo, K., Pasquini, L., Girardi, L., et al. 2007, *A&A*, 475, 981
 Bonfils, X., Delfosse, X., Udry, S., et al. 2013, *A&A*, 549, A109
 Boss, A. P. 1997, *Science*, 276, 1836
 Boss, A. P. 2002, *ApJ*, 576, 462
 Boss, A. P. 2006, *ApJ*, 644, L79
 Brewer, J. M., Fischer, D. A., Valenti, J. A., & Piskunov, N. 2016, *The Astrophysical Journal Supplement Series*, 225, 32
 Brown, A. G. A., Vallenari, A., Prusti, T., et al. 2018, *A&A*, 616, A1
 Buchhave, L. A., Bitsch, B., Johansen, A., et al. 2018, *ApJ*, 856, 37
 Buchhave, L. A., Latham, D. W., Johansen, A., et al. 2012, *Nature*, 486, 375
 Butler, R. P., Vogt, S. S., Marcy, G. W., et al. 2004, *ApJ*, 617, 580
 Carney, B. W., Laird, J. B., Latham, D. W., & Aguilar, L. A. 1996, *AJ*, 112, 668
 Carolo, E., Desidera, S., Gratton, R., et al. 2014, *A&A*, 567, A48
 Cosentino, R., Lovis, C., Pepe, F., et al. 2012, in *Ground-based and Airborne Instrumentation for Astronomy IV*, Vol. 8446, 84461V
 Courcol, B., Bouchy, F., & Deleuil, M. 2016, *MNRAS*, 461, 1841
 Covino, E., Esposito, M., Barbieri, M., et al. 2013, *A&A*, 554, A28
 Cutri, R. M., Skrutskie, M. F., van Dyk, S., et al. 2003, *VizieR Online Data Catalog*, II/246
 da Silva, L., Girardi, L., Pasquini, L., et al. 2006, *A&A*, 458, 609
 Damasso, M., Biazzo, K., Bonomo, A. S., et al. 2015, *A&A*, 575
 Desidera, S., Bonomo, A. S., Claudi, R. U., et al. 2014, *A&A*, 567, L6
 Desidera, S., Sozzetti, A., Bonomo, A. S., et al. 2013, *A&A*, 554, A29
 Dumusque, X., Lovis, C., Ségransan, D., et al. 2011, *A&A*, 535, A55
 Eastman, J., Gaudi, B. S., & Agol, E. 2013, *PASP*, 125, 83
 Endl, M., Brugamyer, E. J., Cochran, W. D., et al. 2016, *ApJ*, 818, 34
 Figueira, P., Santos, N. C., Pepe, F., Lovis, C., & Nardetto, N. 2013, *A&A*, 557
 Figueira, P., Santos, N. C., Pepe, F., Lovis, C., & Nardetto, N. 2015, *A&A*, 582
 Fischer, D. A. & Valenti, J. 2005, *ApJ*, 622, 1102
 Gaia Collaboration, Prusti, T., de Bruijne, J. H. J., et al. 2016, *A&A*, 595, A1
 Gonzalez, G. 1997, *MNRAS*, 285, 403
 Gonzalez, G. 2014, *MNRAS*, 443, 393
 Haywood, M. 2008, *A&A*, 482, 673
 Haywood, M. 2009, *ApJ*, 698, L1
 Ida, S. & Lin, D. N. C. 2004, *ApJ*, 616, 567
 Johnson, J. A., Aller, K. M., Howard, A. W., & Crepp, J. R. 2010, *Publications of the Astronomical Society of the Pacific*, 122, 905
 Johnson, J. A., Butler, R. P., Marcy, G. W., et al. 2007, *ApJ*, 670, 833
 Johnson, J. L. & Li, H. 2012, *ApJ*, 751, 81
 Johnson, M. C., Endl, M., Cochran, W. D., et al. 2016, *ApJ*, 821, 74
 Jones, M. I. & Jenkins, J. S. 2014, *A&A*, 562, A129
 Kang, W., Lee, S.-G., & Kim, K.-M. 2011, *ApJ*, 736, 87
 Kurucz, R. L. 1993, in *Astronomical Society of the Pacific Conference Series*, Vol. 44, IAU Colloq. 138: Peculiar versus Normal Phenomena in A-type and Related Stars, ed. M. M. Dworetsky, F. Castelli, & R. Faraggiana, 87
 Lanza, A. F., Malavolta, L., Benatti, S., et al. 2018, *A&A*, 616, A155
 Lanza, A. F., Molaro, P., Monaco, L., & Haywood, R. D. 2016, *A&A*, 587, A103
 Lovis, C., Dumusque, X., Santos, N. C., et al. 2011, *ArXiv e-prints* [arXiv:1107.5325]
 Maldonado, J., Affer, L., Micela, G., et al. 2015a, *A&A*, 577, A132
 Maldonado, J., Eiroa, C., Villaver, E., Montesinos, B., & Mora, A. 2015b, *A&A*, 579, A20

- Maldonado, J., Villaver, E., & Eiroa, C. 2018, A&A, 612, A93
- Mamajek, E. E. & Hillenbrand, L. A. 2008, ApJ, 687, 1264
- Mayer, L., Quinn, T., Wadsley, J., & Stadel, J. 2002, Science, 298, 1756
- Mayor, M., Marmier, M., Lovis, C., et al. 2011, ArXiv e-prints [arXiv:1109.2497]
- Mayor, M., Pepe, F., Queloz, D., et al. 2003, The Messenger, 114, 20
- Mints, A. & Hekker, S. 2017, A&A, 604, A108
- Monet, D. G., Levine, S. E., Canzian, B., et al. 2003, AJ, 125, 984
- Mordasini, C., Alibert, Y., & Benz, W. 2009, A&A, 501, 1139
- Mordasini, C., Alibert, Y., Benz, W., Klahr, H., & Henning, T. 2012, A&A, 541, A97
- Mortier, A., Santos, N. C., Sousa, S. G., et al. 2013, A&A, 557, A70
- Mortier, A., Santos, N. C., Sozzetti, A., et al. 2012, A&A, 543, A45
- Mulders, G. D., Pascucci, I., Apai, D., Frasca, A., & Molenda-Žakowicz, J. 2016, AJ, 152, 187
- Müller, A., Roccatagliata, V., Henning, T., et al. 2013, A&A, 556, A3
- Nardetto, N., Mourard, D., Kervella, P., et al. 2006, A&A, 453, 309
- Noyes, R. W., Hartmann, L. W., Baliunas, S. L., Duncan, D. K., & Vaughan, A. H. 1984, ApJ, 279, 763
- Pollack, J. B., Hubickyj, O., Bodenheimer, P., et al. 1996, Icarus, 124, 62
- Robertson, P., Endl, M., Cochran, W. D., et al. 2012, ApJ, 749, 39
- Ryan, S. G. 1989, AJ, 98, 1693
- Ryan, S. G. & Norris, J. E. 1991, AJ, 101, 1835
- Saar, S. H., Butler, R. P., & Marcy, G. W. 1998, ApJ, 498, L153
- Saar, S. H. & Donahue, R. A. 1997, ApJ, 485, 319
- Saar, S. H. & Fischer, D. 2000, ApJ, 534, L105
- Santos, N. C., Adibekyan, V., Figueira, P., et al. 2017, A&A, 603, A30
- Santos, N. C., Gomes da Silva, J., Lovis, C., & Melo, C. 2010a, A&A, 511, A54
- Santos, N. C., Israelian, G., & Mayor, M. 2001, A&A, 373, 1019
- Santos, N. C., Israelian, G., & Mayor, M. 2004, A&A, 415, 1153
- Santos, N. C., Mayor, M., Benz, W., et al. 2010b, A&A, 512, A47
- Santos, N. C., Mayor, M., Bonfils, X., et al. 2011, A&A, 526, A112
- Santos, N. C., Mayor, M., Bouchy, F., et al. 2007, A&A, 474, 647
- Santos, N. C., Mayor, M., Naef, D., et al. 2002, A&A, 392, 215
- Santos, N. C., Sousa, S. G., Mortier, A., et al. 2013, A&A, 556, A150
- Smart, R. L. & Nicastro, L. 2014, A&A, 570, A87
- Snedden, C. 1973, ApJ, 184, 839
- Soubiran, C. & Girard, P. 2005, A&A, 438, 139
- Sousa, S. G., Santos, N. C., Adibekyan, V., Delgado- Mena, E., & Israelian, G. 2015, A&A, 577, A67
- Sousa, S. G., Santos, N. C., Israelian, G., Mayor, M., & Udry, S. 2011, A&A, 533
- Sousa, S. G., Santos, N. C., Mayor, M., et al. 2008, A&A, 487, 373
- Sozzetti, A. 2004, MNRAS, 354, 1194
- Sozzetti, A., Torres, G., Charbonneau, D., et al. 2007, ApJ, 664, 1190
- Sozzetti, A., Torres, G., Latham, D. W., et al. 2006, ApJ, 649, 428
- Sozzetti, A., Torres, G., Latham, D. W., et al. 2009, ApJ, 697, 544
- Tody, D. 1993, in Astronomical Data Analysis Software and Systems II, ed. R. J. Hanisch, R. J. V. Brissenden, & J. Barnes, Vol. 52, 173
- Torres, G. 1999, Publications of the Astronomical Society of the Pacific, 111, 169
- Torres, G., Fischer, D. A., Sozzetti, A., et al. 2012, ApJ, 757, 161
- Tsantaki, M., Sousa, S. G., Adibekyan, V. Z., et al. 2013, A&A, 555, A150
- Udry, S., Mayor, M., Benz, W., et al. 2006, A&A, 447, 361
- Yi, S. K., Kim, Y.-C., Demarque, P., et al. 2008, in IAU Symposium, Vol. 252, The Art of Modeling Stars in the 21st Century, ed. L. Deng & K. L. Chan, 413–416
- Zechmeister, M. & Kürster, M. 2009, A&A, 496, 577

Table 5. HARPS-N measurements for HD 220197 and HD 233832

BJD	T_{exp} [s]	RV [kms $^{-1}$]	BIS [kms $^{-1}$]	FWHM [kms $^{-1}$]	$\log R'_{HK}$	Air mass
HD 220197						
2456166.694961	900	-40.2310 ± 0.0007	-0.024	6.409 (6.405)	-4.976	1.24
2456174.590436	600	-40.2275 ± 0.0006	-0.024	6.400 (6.395)	-4.985	1.03
2456175.648876	600	-40.2314 ± 0.0008	-0.024	6.404 (6.399)	-4.974	1.15
2456180.609609	600	-40.2322 ± 0.0007	-0.029	6.411 (6.405)	-4.967	1.08
2456181.622981	600	-40.2602 ± 0.0041	-0.021	6.407	-4.988	1.02
2456198.602376	900	-40.2287 ± 0.0014	-0.022	6.386 (6.377)	-4.774	1.22
2456201.600188	600	-40.2235 ± 0.0010	-0.019	6.385 (6.375)	-4.848	1.24
2456295.310855	600	-40.2369 ± 0.0007	-0.023	6.440 (6.413)	-4.974	1.13
2456298.304272	600	-40.2333 ± 0.0009	-0.019	6.432 (6.405)	-4.986	1.14
2456299.306391	600	-40.2356 ± 0.0007	-0.020	6.443 (6.415)	-4.968	1.16
2456305.355553	600	-40.2273 ± 0.0007	-0.023	6.434 (6.405)	-4.984	1.58
2456322.303008	600	-40.2312 ± 0.0010	-0.017	6.336 (6.304)	-4.926	1.53
2456324.308237	600	-40.2338 ± 0.0023	-0.016	6.353 (6.320)	-4.862	1.65
2456324.321974	1256	-40.2376 ± 0.0012	-0.023	6.442 (6.410)	-4.959	1.90
2456483.729524	600	-40.2306 ± 0.0008	-0.020	6.458 (6.391)	-4.970	1.02
2456484.650796	600	-40.2385 ± 0.0009	-0.020	6.469 (6.402)	-4.966	1.11
2456485.727683	600	-40.2362 ± 0.0007	-0.020	6.467 (6.401)	-4.964	1.02
2456486.702419	600	-40.2325 ± 0.0007	-0.021	6.466 (6.399)	-4.953	1.02
2456487.721348	600	-40.2358 ± 0.0010	-0.020	6.475 (6.408)	-4.931	1.02
2456506.574807	600	-40.2325 ± 0.0010	-0.027	6.473 (6.401)	-4.952	1.16
2456530.649056	600	-40.2395 ± 0.0007	-0.025	6.481 (6.404)	-4.963	1.07
2456531.651444	600	-40.2343 ± 0.0007	-0.025	6.480 (6.403)	-4.962	1.09
2456532.735569	600	-40.2390 ± 0.0007	-0.027	6.483 (6.405)	-4.953	1.53
2456543.454059	600	-40.2369 ± 0.0008	-0.024	6.481 (6.401)	-4.961	1.25
2456544.661037	600	-40.2350 ± 0.0007	-0.023	6.474 (6.394)	-4.968	1.24
2456563.661916	600	-40.2365 ± 0.0008	-0.023	6.476 (6.391)	-4.966	1.64
2456565.619851	600	-40.2381 ± 0.0006	-0.022	6.484 (6.399)	-4.971	1.33
2456566.606976	600	-40.2385 ± 0.0007	-0.027	6.485 (6.399)	-4.960	1.27
2456579.602415	600	-40.2355 ± 0.0007	-0.017	6.480 (6.391)	-4.976	1.49
2456585.575694	600	-40.2373 ± 0.0008	-0.025	6.483 (6.392)	-4.976	1.40
2456602.563242	600	-40.1661 ± 0.0004	0.026	6.352	-5.000	1.76
2456975.415640	600	-40.2321 ± 0.0007	-0.023	6.401	-4.976	1.05
2456998.337040	600	-40.2360 ± 0.0008	-0.024	6.404	-4.984	1.03
2456999.318083	600	-40.2360 ± 0.0009	-0.021	6.400	-4.978	1.02
2457002.320534	1200	-40.2376 ± 0.0018	-0.026	6.413	-4.960	1.03
2457003.323066	599	-40.2442 ± 0.0010	-0.020	6.404	-4.990	1.03
2457004.303645	600	-40.2346 ± 0.0009	-0.024	6.404	-5.002	1.02
2457023.326190	600	-40.2368 ± 0.0014	-0.028	6.405	-5.023	1.16
2457259.522203	600	-40.2341 ± 0.0007	-0.021	6.398	-4.961	1.14
2457269.670182	600	-40.2347 ± 0.0008	-0.022	6.402	-4.946	1.21
2457270.647244	600	-40.2329 ± 0.0006	-0.024	6.403	-4.957	1.13
2457271.679872	600	-40.2338 ± 0.0007	-0.023	6.404	-4.960	1.29
2457272.688865	600	-40.2343 ± 0.0007	-0.024	6.401	-4.954	1.36
2457273.623433	600	-40.2325 ± 0.0008	-0.018	6.402	-4.958	1.09
2457290.535927	600	-40.2321 ± 0.0009	-0.021	6.398	-4.966	1.03
2457291.504218	600	-40.2307 ± 0.0007	-0.022	6.399	-4.970	1.02
2457611.684273	600	-40.2303 ± 0.0009	-0.024	6.398	-4.967	1.07
2457623.530276	600	-40.2265 ± 0.0008	-0.017	6.391	-4.986	1.12
2457624.498685	600	-40.2323 ± 0.0008	-0.021	6.396	-4.978	1.23
2457644.645211	600	-40.2359 ± 0.0008	-0.021	6.401	-4.962	1.22
2457651.646254	600	-40.2287 ± 0.0007	-0.021	6.396	-4.968	1.33
2457652.647862	600	-40.2330 ± 0.0009	-0.023	6.397	-4.986	1.35
2457653.641366	600	-40.2329 ± 0.0008	-0.021	6.394	-4.972	1.33
2457654.644151	600	-40.2352 ± 0.0011	-0.025	6.406	-4.990	1.37
2457665.542415	600	-40.2289 ± 0.0007	-0.024	6.395	-4.971	1.07
2457679.563255	600	-40.2288 ± 0.0008	-0.027	6.401	-4.961	1.29
2457680.497913	600	-40.2276 ± 0.0007	-0.021	6.391	-4.984	1.07
2457681.537819	600	-40.2286 ± 0.0007	-0.019	6.394	-4.990	1.19
2457683.571934	600	-40.2279 ± 0.0008	-0.017	6.394	-4.684	1.42

Table 5. continued.

BJD	T_{exp} [s]	RV [kms ⁻¹]	BIS [kms ⁻¹]	FWHM [kms ⁻¹]	$\log R'_{HK}$	Air mass
2457701.573526	600	-40.2304 ± 0.0018	-0.029	6.409	-4.970	2.11
2457702.474375	600	-40.2338 ± 0.0014	-0.026	6.405	-5.008	1.17
2457727.401991	600	-40.2281 ± 0.0007	-0.021	6.395	-5.000	1.17
2457749.342299	600	-40.2310 ± 0.0009	-0.024	6.399	-4.987	1.17
2457750.357793	600	-40.2353 ± 0.0013	-0.024	6.394	-5.002	1.26
2457936.674180	600	-40.2330 ± 0.0010	-0.023	6.396	-4.970	1.11
2457937.674293	600	-40.2289 ± 0.0009	-0.021	6.396	-4.981	1.10
2457942.698513	600	-40.2276 ± 0.0009	-0.021	6.394	-4.975	1.04
2457943.725246	600	-40.2297 ± 0.0008	-0.017	6.391	-4.975	1.02
2457944.596109	600	-40.2328 ± 0.0009	-0.022	6.398	-4.971	1.37
2457952.703357	600	-40.2354 ± 0.0011	-0.020	6.399	-4.984	1.02
2457953.688599	600	-40.2335 ± 0.0009	-0.020	6.402	-4.963	1.02
2457954.694734	600	-40.2341 ± 0.0008	-0.022	6.401	-4.971	1.02
2457956.654577	600	-40.2338 ± 0.0009	-0.023	6.395	-4.980	1.04
2457971.637507	600	-40.2334 ± 0.0008	-0.021	6.395	-4.975	1.02
2457972.552032	600	-40.2337 ± 0.0011	-0.015	6.393	-4.968	1.20
2457973.660713	1800	-40.2327 ± 0.0007	-0.027	6.391	-4.980	1.03
2457974.592877	600	-40.2330 ± 0.0010	-0.018	6.400	-4.969	1.07
2457984.623067	600	-40.2282 ± 0.0009	-0.023	6.396	-4.985	1.02
2457989.541598	600	-40.2311 ± 0.0008	-0.018	6.401	-4.976	1.09
2457991.590650	600	-40.2283 ± 0.0014	-0.019	6.400	-4.967	1.02
2457993.596882	600	-40.2289 ± 0.0008	-0.021	6.397	-4.963	1.02
2457996.547027	600	-40.2350 ± 0.0019	-0.024	6.390	-5.048	1.04
2457997.502323	600	-40.2284 ± 0.0012	-0.021	6.395	-4.972	1.14
2458024.567725	600	-40.2351 ± 0.0007	-0.026	6.399	-4.962	1.09
2458026.634837	600	-40.2332 ± 0.0014	-0.021	6.399	-4.976	1.44
2458027.533479	1200	-40.2336 ± 0.0019	-0.022	6.401	-4.972	1.05
2458031.545700	600	-40.2303 ± 0.0009	-0.024	6.401	-4.979	1.09
2458044.476041	600	-40.2338 ± 0.0008	-0.016	6.396	-4.965	1.03
HD 233832						
2456344.717204	900	-65.5142 ± 0.0007	0.007	5.735 (5.660)	-4.934	1.25
2456363.624524	900	-65.5192 ± 0.0008	0.011	5.721 (5.656)	-4.942	1.14
2456364.633696	900	-65.5173 ± 0.0009	0.006	5.720 (5.655)	-4.963	1.17
2456375.538791	900	-65.5146 ± 0.0013	0.012	5.717 (5.655)	-4.992	1.08
2456376.484746	900	-65.5150 ± 0.0009	0.008	5.722 (5.659)	-4.992	1.09
2456380.557851	900	-65.5165 ± 0.0011	0.001	5.727 (5.665)	-4.981	1.11
2456381.614271	900	-65.5162 ± 0.0008	0.006	5.721 (5.659)	-4.980	1.25
2456381.626365	900	-65.5175 ± 0.0008	0.004	5.725 (5.662)	-4.989	1.29
2456405.551638	900	-65.5135 ± 0.0015	0.013	5.722 (5.654)	-4.957	1.26
2456410.578812	900	-65.5291 ± 0.0020	-0.007	5.719 (5.648)	-4.975	1.47
2456424.522687	900	-65.5144 ± 0.0009	0.007	5.741 (5.660)	-5.011	1.37
2457097.533774	900	-65.4442 ± 0.0013	-0.001	5.652	-4.978	1.08
2457099.561761	900	-65.4451 ± 0.0012	-0.005	5.647	-4.988	1.08
2457108.698979	900	-65.4508 ± 0.0044	0.014	5.664	-4.773	1.70
2457109.471016	900	-65.4425 ± 0.0012	0.009	5.665	-4.972	1.10
2457110.444016	900	-65.4387 ± 0.0031	0.020	5.654	-4.874	1.13
2457112.440808	900	-65.4433 ± 0.0030	0.016	5.666	-4.841	1.12
2457113.454520	900	-65.4439 ± 0.0010	0.009	5.661	-4.994	1.10
2457114.407702	900	-65.4425 ± 0.0020	0.008	5.661	-4.929	1.18
2457137.358615	900	-65.4429 ± 0.0013	0.006	5.661	-5.004	1.15
2457142.478326	900	-65.4430 ± 0.0011	0.002	5.665	-4.992	1.12
2457143.410021	900	-65.4429 ± 0.0009	0.004	5.659	-4.986	1.08
2457144.439637	900	-65.4410 ± 0.0009	0.010	5.668	-4.974	1.08
2457145.437333	900	-65.4422 ± 0.0015	0.010	5.665	-4.970	1.08
2457154.430419	900	-65.4378 ± 0.0023	0.006	5.653	-4.987	1.10
2457169.406042	900	-65.4451 ± 0.0012	0.009	5.663	-5.010	1.13
2457170.403782	900	-65.4431 ± 0.0009	0.006	5.659	-4.986	1.13
2457205.386928	900	-65.4469 ± 0.0008	0.012	5.659	-4.996	1.40
2457209.382307	900	-65.4488 ± 0.0017	0.013	5.663	-4.966	1.44
2457353.700256	1200	-65.4538 ± 0.0021	0.002	5.662	-4.945	1.36

Table 5. continued.

BJD	T_{exp} [s]	RV [kms ⁻¹]	BIS [kms ⁻¹]	FWHM [kms ⁻¹]	$\log R'_{HK}$	Air mass
2457355.757480	1800	-65.4618 ± 0.0027	0.012	5.673	-4.976	1.14
2457386.668107	900	-65.4592 ± 0.0013	0.018	5.666	-5.001	1.17
2457387.723213	900	-65.4528 ± 0.0013	-0.003	5.656	-4.988	1.08
2457388.738421	900	-65.4588 ± 0.0009	0.005	5.660	-5.004	1.08
2457389.719007	900	-65.4570 ± 0.0013	0.010	5.656	-4.973	1.08
2457391.743411	900	-65.4577 ± 0.0013	0.006	5.667	-4.982	1.08
2457417.741357	1800	-65.4574 ± 0.0026	0.004	5.647	-4.922	1.16
2457418.738511	1800	-65.4692 ± 0.0025	0.002	5.648	-4.928	1.16
2457421.757626	900	-65.4616 ± 0.0025	0.019	5.658	-4.932	1.22
2457443.585531	900	-65.4636 ± 0.0017	0.017	5.655	-4.963	1.08
2457444.579873	900	-65.4694 ± 0.0034	0.007	5.669	-5.014	1.08
2457445.517548	900	-65.4651 ± 0.0013	0.013	5.659	-5.021	1.15
2457472.514832	900	-65.4662 ± 0.0012	0.012	5.663	-5.042	1.07
2457475.508171	900	-65.4685 ± 0.0017	0.007	5.652	-5.068	1.07
2457491.397269	900	-65.4672 ± 0.0009	0.009	5.659	-5.025	1.13
2457492.393470	900	-65.4662 ± 0.0011	0.004	5.660	-5.046	1.14
2457501.482698	900	-65.4685 ± 0.0010	0.003	5.654	-5.029	1.10
2457513.505807	900	-65.4666 ± 0.0012	0.009	5.659	-5.029	1.23
2457521.469448	900	-65.4629 ± 0.0010	0.014	5.658	-5.045	1.19
2457522.384150	900	-65.4690 ± 0.0013	0.009	5.662	-5.043	1.08
2457523.426551	900	-65.4722 ± 0.0033	-0.001	5.659	-5.149	1.11
2457525.399486	900	-65.4712 ± 0.0015	0.004	5.652	-5.088	1.09
2457526.405188	900	-65.4683 ± 0.0011	0.010	5.663	-5.058	1.10
2457540.378563	900	-65.4718 ± 0.0011	0.017	5.664	-5.032	1.11
2457552.387606	900	-65.4725 ± 0.0021	0.006	5.662	-5.096	1.20
2457553.396578	900	-65.4720 ± 0.0015	0.007	5.650	-5.042	1.23
2457573.391404	900	-65.4727 ± 0.0009	0.006	5.658	-5.043	1.47
2457574.382765	900	-65.4727 ± 0.0013	0.008	5.649	-5.063	1.44
2457703.767152	900	-65.4826 ± 0.0012	0.003	5.660	-5.041	1.26
2457763.587833	900	-65.4860 ± 0.0015	0.000	5.655	-5.067	1.33
2457773.685240	900	-65.4816 ± 0.0013	0.008	5.657	-5.033	1.08
2457790.737442	900	-65.4862 ± 0.0010	0.005	5.659	-5.031	1.19
2457808.567046	900	-65.4873 ± 0.0010	0.013	5.657	-5.058	1.09
2457810.564248	900	-65.4883 ± 0.0028	0.004	5.666	-5.115	1.08
2457812.620392	900	-65.4854 ± 0.0010	0.005	5.653	-5.027	1.09
2457833.458789	900	-65.4896 ± 0.0017	0.005	5.655	-5.006	1.14
2457852.540479	900	-65.4910 ± 0.0016	0.010	5.656	-4.992	1.13
2457853.541938	900	-65.4907 ± 0.0022	0.010	5.657	-5.103	1.14
2457862.448992	900	-65.4888 ± 0.0010	0.013	5.666	-5.057	1.07
2457895.461297	900	-65.4914 ± 0.0010	0.011	5.656	-5.035	1.23
2457932.386154	900	-65.4927 ± 0.0041	0.002	5.665	-5.009	1.35
2457933.398122	900	-65.4976 ± 0.0035	0.009	5.662	-5.012	1.42
2457934.397580	900	-65.4947 ± 0.0041	0.011	5.661	-5.004	1.44
2457935.393821	900	-65.4943 ± 0.0061	0.004	5.656	-5.021	1.43
2458047.760373	900	-65.4990 ± 0.0025	0.004	5.656	-5.114	1.61
2458075.754804	900	-65.5039 ± 0.0012	0.013	5.655	-5.132	1.24
2458189.733233	900	-65.5064 ± 0.0011	0.005	5.652	-5.114	1.64
2458190.690636	900	-65.5087 ± 0.0010	0.004	5.659	-5.118	1.37
2458268.439049	1800	-65.5074 ± 0.0018	0.005	5.666	-5.107	1.25
2458269.473627	900	-65.5076 ± 0.0009	0.005	5.664	-5.050	1.39